
Hamiltonian latent operators for content and motion disentanglement in image sequences

Asif Khan

School of Informatics
University of Edinburgh
asif.khan@ed.ac.uk

Amos Storkey

School of Informatics
University of Edinburgh
a.storkey@ed.ac.uk

Abstract

We introduce *HALO* – a deep generative model utilising HAmiltonian Latent Operators to reliably disentangle content and motion information in image sequences. The *content* represents summary statistics of a sequence, and *motion* is a dynamic process that determines how information is expressed in any part of the sequence. By modelling the dynamics as a Hamiltonian motion, important desiderata are ensured: (1) the motion is reversible, (2) the symplectic, volume-preserving structure in phase space means paths are continuous and are not divergent in the latent space. Consequently, the nearness of sequence frames is realised by the nearness of their coordinates in the phase space, which proves valuable for disentanglement and long-term sequence generation. The sequence space is generally comprised of different types of dynamical motions. To ensure long-term separability and allow controlled generation, we associate every motion with a unique Hamiltonian that acts in its respective subspace. We demonstrate the utility of *HALO* by swapping the motion of a pair of sequences, controlled generation, and image rotations.

1 Introduction

The ability to learn to generate artificial image sequences has diverse uses, from animation, keyframe generation, and summarisation to restoration that has been explored in previous work over many decades (Hogg, 1983; Hurri and Hyvärinen, 2003; Cremers and Yuille, 2003; Storkey and Williams, 2003; Kannan et al., 2005). However, learning to generate arbitrary sequences is not enough; to hold a practical application, the user must be able to control aspects of the sequence generation, such as the motion being enacted or the characteristics of the agent doing an action. To enable this, we must learn to decompose image sequences into *content* and *motion* characteristics so that we can apply learnt motions to new objects or vary the motions being applied.

Deep generative models (DGMs) such as variational autoencoders (VAEs) (Kingma and Welling, 2013) and Generative Adversarial Networks (GANs) (Goodfellow et al., 2014) use neural networks (NNs) to transform the samples from a prior distribution over lower-dimensional latent factors to samples from the data distribution itself. Recent developments (Chung et al., 2015; Srivastava et al., 2015; Hsu et al., 2017; Yingzhen and Mandt, 2018) extend VAEs to sequences using Recurrent Neural Networks (RNNs) on the representation of temporal frames. Similar approaches have been taken for GAN models (Tulyakov et al., 2018; Yoon et al., 2019; Dandi et al., 2020).

The dynamical processes creating the evolution of image sequences are highly constrained. Consider the simplistic case of a person walking in a scene with a camera moving around that individual. The walking pose will return to similar positions periodically, and likewise, the revolving camera will revisit previous positions. Even without strict periodicity, many dynamical processes are reversible. Any time that a dynamic could conceivably return to an earlier state suggests an implicit conservation law—the conservation of information in the underlying scene generator—as it must be capable of

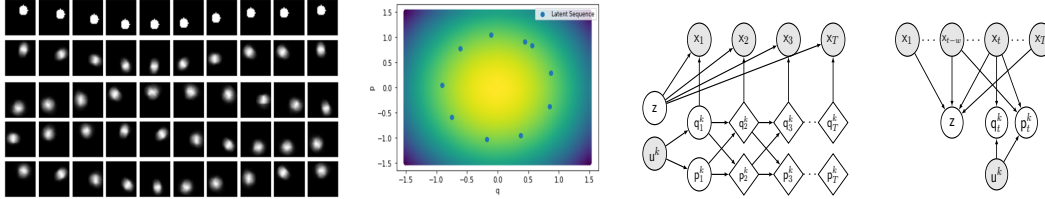


Figure 1: Left: we empirically demonstrate the benefits of learning Hamiltonian operator in the latent space. Consider $(32, 32)$ image sequence of a ball rotating in a fixed orbit; the (i, j) centre of a ball moves under constraint $i^2 + j^2 = c$, where c is a constant. We generated a data set of sequences with different initial condition and same number of time steps. Next, we trained a VAE with Hamiltonian operator in the latent space. We use an encoder to transform sequences to a 2-dimensional phase space, next we unroll a trajectory using a learnable Hamiltonian operator and finally use decoder to obtain the sequence. Top row is the original sequence, second row is the reconstructed sequence and below are three sequences generated from random initial states. Middle: the coordinates in the phase space are coloured by the energy value, alongwith a representation of a sequence generated from a random initial coordinate. Right: is the probabilistic graph of our generative and inference model.

returning to and regenerating the same scene with non-negligible probability. The critical observation we wish to capture in this paper is that understanding the conservation occurring in the context of a set of sequences is a vital ingredient to decomposing *content* from *motion*.

Given any conserved quantity, any motion must be modelled to maintain the conserved quantity. In physics, such a motion is called a *Hamiltonian* motion; it keeps the corresponding Hamiltonian function constant. Hence we argue that a flexible latent Hamiltonian model provides a good inductive bias to learn a representation space that enables conservation of the right quantities (which are themselves learnt) and models the dynamic evolution. This is mathematically equivalent to saying that we can learn to represent the underlying motions as combinations of differentiable symmetry groups; all differentiable symmetry transformations follow a conservation law (Noether, 1918).

We next illustrate the benefit of using Hamiltonian dynamics in the latent space of DGM in Figure 1.¹ Here, we observe using the Hamiltonian dynamics model can discover constant energy in latent space from a set of image sequences proving critical for generating novel energy preserving sequences. This example demonstrates identifying symmetries is a suitable inductive bias for developing expressive DGMs that understand the motion constraints and generalise beyond the training data. Higgins et al. (2018); Toth et al. (2019); Botev et al. (2021) have discussed the benefits of such inductive biases for learning disentangled representation.

The existing sequential DGMs do not impose any structural prior for constraining the dynamics in motion space and, therefore, accumulate errors as the sequence length grows, quickly deviating from the relevant path (Karl et al., 2016; Fraccaro et al., 2017; Yildiz et al., 2019; Bird and Williams, 2019). The attractive property of Hamiltonian dynamics is that they are *symplectic* that is, the divergence of a vector field is zero, and the evolving dynamics preserve the infinitesimal volume element. Consequently, the motion paths are restricted to a low-dimensional manifold in the latent space, and we can predict the dynamics forward and backwards in time.

In this paper, we intimate the more general applicability of latent Hamiltonian models; previous applications have been limited to somewhat constrained physical systems. We propose *HALO* – a VAE framework to model the dynamics of image sequences using a collection of learnable linear Hamiltonian operators in the latent space. Specifically, for any motion sequence, we model the transition from a time step t to a step $t + 1$ using a group action of a Hamiltonian operator. The evolution of the dynamics of a sequence leaves certain information unchanged, identified as *content*, and specific properties that evolve in conjunction (i.e. *motion*). Since the space of image sequences can comprise various types of dynamical actions, we split the *motion space* into subspaces where each subspace models a unique action and is unaffected by other actions. This formulation explicitly ensures the separability of dynamics. It further reduces the computational cost since the Hamiltonian of the space is now in a block diagonal form where each block is a Hamiltonian of a symmetry subgroup. Here, we focus on a discrete, identified set of actions that we can then compose at generation time. We want to remark our method can also work without action labels,

¹We discuss the specifics of dynamical operators in Section 3

as empirically demonstrated in the results. The benefit of identifying actions apriori is that we can use it for a controlled generation. We empirically demonstrate the advantages of our approach through i) generation of diverse dynamics from a starting frame and ii) demonstrating successful disentanglement of the content and motion representation.

2 Related Work

Hamiltonian Neural Networks Several deep learning (DL) methods have recently been proposed to learn the dynamics of physical systems using Hamiltonian mechanics. Greydanus et al. (2019) use NNs to predict Hamiltonian from phase-space coordinates $\mathbf{s} = (\mathbf{p}, \mathbf{q})$ and their derivatives. In similar work (Bondesan and Lamacraft, 2019) used NNs to discover symmetries of Hamiltonian mechanical systems. More recently, Hamiltonian NNs have been used for simulating complex physical systems (Sanchez-Gonzalez et al., 2019, 2020). The key idea of this work is to represent the states of particles as a graph and use a graph neural network (GNN) to predict the change from the current state to the next state. In a follow-up Cranmer et al. (2020), introduce sparsity on the messages in a graph and use the symbolic regression method to search for physical laws that describe the messages in the graph. Recently Toth et al. (2019) developed the Hamiltonian generative network (HGN), where they proposed to learn a Hamiltonian from image sequences. HGN maps a sequence to a latent representation and then projects it to the phase space to unroll the dynamics using a symplectic ODE integrator with Hamilton’s equation. In another work Yildiz et al. (2019) use second-order ODE parameterised as a BNN for modelling dynamics of high dimensional sequence data in the latent space of VAE. Most of the developments are built on the neural ODE (Chen et al., 2018), an idea to view layers of NNs as internal states of an ODE. These methods rely on the numerical integration scheme and the stability of the ODE solver. A Hamiltonian formalism dictates an additional requirement that the dynamics of an ODE should be volume-preserving and reversible. We want to clarify that, unlike HGN, which mainly focuses on sequence generation and relies on symplectic ODE integrators in the latent space, we use linear Hamiltonian operators with matrix exponentials and demonstrate its relevance for disentanglement.

Latent Space Models There is a long history of latent state space models for modelling sequences (Kalman, 1960; Starnier and Pentland, 1997; Roweis and Ghahramani, 1999; Elliott and Krishnamurthy, 1999; Pavlovic et al., 2000). More recently, these methods have been combined with deep generative models for generating high dimensional sequences as well as learning a disentangled representation (Karl et al., 2016; Villegas et al., 2017; Tulyakov et al., 2018; Hsieh et al., 2018; Yingzhen and Mandt, 2018; Miladinović et al., 2019; Minderer et al., 2019; Franceschi et al., 2020; Zhu et al., 2020). MoCoGAN (Tulyakov et al., 2018) developed an adversarial framework, combining a random content noise with a sequence of random motion noise to generate videos. More recently, DSVAE (Yingzhen and Mandt, 2018) proposed to split a latent space into time-variant and invariant representations and use LSTM (Hochreiter and Schmidhuber, 1997) to learn the prior on time-variant representation. S3VAE (Zhu et al., 2020) improves the disentanglement of DSVAE by minimising a mutual information loss between content and motion variables. Some Hamiltonian methods (Toth et al., 2019; Yildiz et al., 2019) also model the dynamics of high dimensional sequential data in a latent space. However, the focus in those cases is only on sequence generation; to our knowledge, this has not been investigated for disentanglement.

Group Transformations in Latent Space Models Rao and Ruderman (1999) proposed the algorithm to model the infinitesimal movement on data manifold using learnable Lie group operators. Culpepper and Olshausen (2009) use the matrix exponents to learn the transport operators for modelling the manifold trajectory. Many other similar methods have investigated the use of geometric operators for learning the manifold representation from data (Rao and Ruderman, 1999; Culpepper and Olshausen, 2009; Memisevic, 2012; Sohl-Dickstein et al., 2010; Cohen and Welling, 2014). The use of symmetries for learning disentangled factors of variations has recently been considered. A disentanglement is generally identified as learning representations with independent latent factors. The main goal is that each latent factor should control a distinct data factor, and a single latent variable should control no two data factors, Various authors (Bengio et al., 2013; Lake et al., 2017; Eastwood and Williams, 2018). Higgins et al. (2018) have proposed a symmetry-based definition of disentanglement. The goal in these settings was to decompose a latent space into subspaces and on each subspace, to learn a unique group transformation such that the subspace is unchanged by the action of other groups. Caselles-Dupré et al. (2019), build such a model using interaction with the

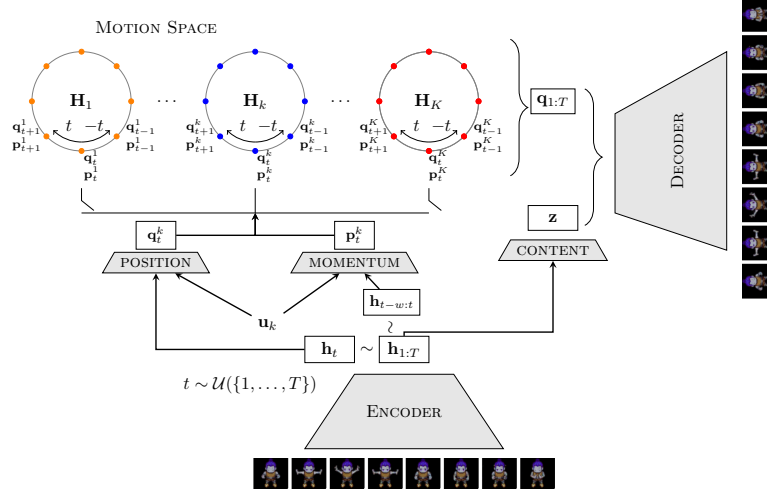


Figure 2: The framework for our model. We first encode each time step of a sequence to a respective feature vector $\mathbf{h}_{1:T}$. Next, to unroll the dynamics of an action k , we map the feature representation to the respective phase space. Specifically, we sample a starting index t and map \mathbf{h}_t to position coordinate \mathbf{q}_t^k . For momentum \mathbf{p}_t^k , we use temporal convolution with a kernel size w on $\mathbf{h}_{t-w:t}$. We then use the operator \mathbf{H}_k to trace out the forward and backward trajectory. At last, we combine the position coordinates of all timesteps $\mathbf{q}_{1:T}$ with the content representation \mathbf{z} and pass it through the decoder network to generate the sequence.

environment. Some other similar approaches were recently proposed to learn group transformations in a latent space (Connor and Rozell, 2020; Quessard et al., 2020; Dupont et al., 2020). However, the applications were restricted to relatively toy problems and, to our knowledge, have not been investigated on higher dimensional videos.

3 Method

Here, we introduce *HALO* for sets of sequential image data. Each set of sequences depicts the temporal evolution associated with one of several *actions*. In this context, an *action* is simply a label associated with a particular sequence set, but where it is understood, the sequences within a set may have very different content but the same dynamic form, e.g. in the sprites data (discussed later) the actions are ‘walking’, ‘spell cast’, and ‘slash’ and the sequences within a set are different individuals performing the relevant action. In the following, we assume the separation into action sets is known, but that assumption is relaxed later.

Let $\mathbf{x}_{1:T}^i$ denote the i th image sequence, with \mathbf{x}_t^i the t th frame in the sequence. Let \mathbf{u}^i be an indicator vector denoting the action associated with the i th sequence; i.e. $u_k^i = 1$ iff sequence i follows action k and $u_{k'}^i = 0$ for all other $k' \neq k$. These sequences and corresponding actions are collected into a dataset $\{(\mathbf{x}_{1:T}^i, \mathbf{u}^i)\}_{i=1}^N$ of size N , where, for the sake of simplicity in description, we assume they all are of same length T . In this paper, we use a latent space to aid the modelling of each sequence and decompose that latent space into two parts, which we call a *content* space (denoted by \mathbf{Z}) and a *motion* space (denoted by \mathbf{S}). As the data comprises sequences of various actions that take different dynamical forms, we further decompose the latent motion space $\mathbf{S} = \mathbf{S}^1 \oplus \mathbf{S}^2 \oplus \dots \oplus \mathbf{S}^K$, with one subspace for each action. In modelling a sequence corresponding to action k , only the subspace \mathbf{S}^k will be allowed to change across the length of that sequence. Each motion subspace is further decomposed into generalised *position* and *momentum* parts: $\mathbf{S}^k = (\mathbf{p}^k, \mathbf{q}^k)$. Only the position component of this phase space is used together with content to create individual images in a sequence generatively. The momentum part *only* affects the dynamics.

The above formulation provides many advantages; it prevents the neural network from leaking constant *content* information via the motion representation, and it ensures the possibility of preserving key conservation quantities that we argue are implicit in the constraints of most motion dynamics. This is discussed further in Paragraph 3. The full framework of our model is illustrated in Figure 2.

We next introduce the generative model, followed by the variational formalism for inference and learning.

Generative Model For completeness we first present the full probabilistic model in (1-4) before describing each component. Each dynamic is categorised by a particular *action* enumerated by k , encoded in an indicator vector \mathbf{u} (i.e. $u_k = 1$ for action k). The generative model is conditioned on this action vector. First, in (1), we sample the *content* variable \mathbf{z} from a prior $p(\mathbf{z})$. The content variable will describe the constant appearance characteristics expressed throughout the sequence. Next, we sample a starting position from a prior $p(\mathbf{q}_1^k)$, and momentum from a prior $p(\mathbf{p}_1^k)$ (we initialise the actions not represented in the sequence to zero). The full state-space representation for the dynamic of action k is then given by $\mathbf{s}_1^k = (\mathbf{p}_1^k, \mathbf{q}_1^k)$. The dynamical model (3,5) then traces out the forward trajectory in the phase space. Finally, we combine the position trajectory with the content representation and use a decoder neural network to get the emission distribution of the data space sequence. In summary,

GIVEN: k denoting action label for a sequence,

$$\mathbf{z} \sim p(\mathbf{z}), \quad \mathbf{q}_1^k \sim \mathcal{N}(\mathbf{0}, \mathbf{I}_d), \quad \mathbf{p}_1^k \sim \mathcal{N}(\mathbf{0}, \mathbf{I}_d), \quad (1)$$

$$\mathbf{s}_1^k = [\mathbf{p}_1^k, \mathbf{q}_1^k], \quad \mathbf{s}_1^{k'} = \mathbf{0}, \quad \forall k' \neq k, \quad (2)$$

$$\mathbf{s}_t^k = f(\mathbf{s}_{t-1}^k; \omega_k, t), \quad \mathbf{s}_t^{k'} = \mathbf{s}_{t-1}^{k'}, \quad \forall t > 1, k' \neq k \quad (3)$$

$$\mathbf{q}_t = [\mathbf{q}_t^1, \dots, \mathbf{q}_t^K], \quad \mathbf{x}_t \sim \mathcal{N}(\mathbf{x}_t | \phi(\mathbf{z}, \mathbf{q}_t), \alpha^2 \mathbf{I}_m), \quad \forall t \quad (4)$$

where d is the dimensionality of k^{th} subspace, m is the dimensionality of data space, f is a dynamical model (5) and ω_k are the parameters of f to be used for the k^{th} subspace. We use an emission distribution that is a spherical Gaussian, with a parameterised mean $\phi(\cdot, \cdot)$, and a covariance $\alpha^2 \mathbf{I}_m$.

Dynamical Model In image sequences, we can view each frame of a sequence as a point in an abstract representation space; the temporal dynamics trace a path connecting the frames forming a 1-submanifold of the image manifold. Most dynamical models either try to capture this geometry deterministically (Srivastava et al., 2015) or probabilistically (Chung et al., 2015; Hsu et al., 2017; Yingzhen and Mandt, 2018) via linear or non-linear state-space models. In either case, small errors in dynamical steps can accumulate and result in a significant deviation from the manifold when unrolling long-term trajectories at inference time (Karl et al., 2016; Fraccaro et al., 2017). Interestingly, Hamiltonian systems alleviate these issues by constraining the dynamics to be symplectic and reversible. The symplectic geometry ensures the dynamics are volume-preserving, preventing any deviation from the manifold, and reversibility is useful in understanding how the state of an object changes under dynamical evolution. By reversing the arrow of time, the object could return to its previous state, this awareness provides a sense of accountability to an object for its actions. In our work, without significant loss of generality, we propose a linear Hamiltonian system in the latent layer, relying on deep neural network mapping to data space to handle all nonlinear aspects. The linearity of dynamics also enhances the interpretability of the dynamics.

Definition 1. A matrix $\mathbf{H} \in \mathbb{R}^{2d \times 2d}$ is an Hamiltonian matrix if $\mathbf{H}^T \mathbf{J} \mathbf{H} = \mathbf{J}$, where \mathbf{J} is a skew-symmetric matrix $\mathbf{J} = \begin{pmatrix} 0 & \mathbf{I}_d \\ -\mathbf{I}_d & 0 \end{pmatrix}$ and \mathbf{I}_d is an identity matrix.

Consider a coordinate vector $\mathbf{s} \in \mathbb{R}^{2d}$ in the phase space \mathbf{S} at a time t that evolves under constant Hamiltonian energy $\mathbf{E} = \frac{1}{2} \mathbf{s}^T \mathbf{M}(t) \mathbf{s}$, where $\mathbf{M}(t)$ is a symmetric matrix. In Hamiltonian mechanics, the coordinates are specified in terms of position \mathbf{q} and momentum \mathbf{p} variables as $\mathbf{s} = (\mathbf{q}, \mathbf{p})$. Using the fact energy \mathbf{E} is constant over time we can express equation of motion as, $\frac{d\mathbf{s}(t)}{dt} = \mathbf{J} \mathbf{M}(t) \mathbf{s}$. Let $\mathbf{H}(t) = \mathbf{J} \mathbf{M}(t)$, we can rewrite the equation of motion as, $\frac{d\mathbf{s}(t)}{dt} = \mathbf{H}(t) \mathbf{s}$. The closed-form solution is given by matrix exponential $\mathbf{s}(t) = e^{t\mathbf{H}} \mathbf{s}(0)$. The matrix exponent has a connection to Lie algebras, and for small t we can interpret $e^{t\mathbf{H}}$ as an infinitesimal transformation of $\mathbf{s}(0)$ under the action of a Lie group of \mathbf{H} . We discuss this further in Appendix ???. For a detailed introduction to the topic, we refer to Chevalley (2016). We use fast Taylor approximation (Bader et al., 2019) to compute matrix exponential that provides a stable solution under matrix norms.

In this work, we consider K Hamiltonians $\mathbf{H}_1, \dots, \mathbf{H}_K$, each acting on a unique subspace of the phase space $\mathbf{S}^1, \mathbf{S}^2, \dots, \mathbf{S}^K$. To unroll the trajectory of motion k , we use the group action defined by

the matrix exponent of the operator \mathbf{H}_k on a starting phase space representation $\mathbf{s}_1^k \in \mathbf{S}^k$ given by,

$$\mathbf{s}_t^k = f(\mathbf{s}_{t-1}^k; \omega_k, t) = e^{t\mathbf{H}_k} \mathbf{s}_{t-1}^k, \forall t > 1; \quad \mathbf{s}_t^{k'} = \mathbf{0}, \quad \forall t, k' \neq k. \quad (5)$$

The backward dynamics can simply be obtained by negating time, i.e. replacing t with $-t$ in the above. We assume all time steps are equally spaced. The above formulation provides an explicit disentanglement of the motion space. It further allows us to parallelise the computation of matrix exponential by leveraging the block diagonal form of \mathbf{H} . Specific to our work, we parameterise a symmetric matrix \mathbf{M}_k and obtain its Hamiltonian matrix as $\mathbf{H}_k = \mathbf{J}\mathbf{M}_k$ where \mathbf{J} is a fixed skew-symmetric matrix as stated in definition (1). The group of such real Hamiltonian matrices form a symplectic Lie group under multiplication $Sp(2d)$ with $2d^2 + d$ independent elements. The symplectic geometry proves useful for long-term sequence generation. We also consider the symplectic orthogonal group $SpO(2d)$ that further restricts the Hamiltonian matrix to a skew-symmetric form with $(d^2 - d)/2$ independent elements. The benefit of this restriction is that the resulting transforms reduce to rotations which is more interpretable. We briefly introduce the details in Appendix ???. For a more comprehensive overview, we refer readers to Easton (1993).

Inference In order to learn the model parameters, we need to infer the distribution over latent variables. We use variational inference to learn the model parameters that leads to maximising the evidence lower bound (ELBO) objective, $\max_q \mathbb{E}_{q(\mathbf{z}, \mathbf{s}_t | \mathbf{x}_{1:T}, \mathbf{u})} \log \left[\frac{p(\mathbf{x}_{1:T}, \mathbf{z}, \mathbf{s}_{1:T} | \mathbf{u})}{q(\mathbf{z}, \mathbf{s}_t | \mathbf{x}_{1:T}, \mathbf{u})} \right]$, where $q(\cdot | \cdot)$ is the approximate posterior distribution and $\mathbf{s}_t = [\mathbf{q}_t^k, \mathbf{p}_t^k]$. It remains to define the approximate posterior we use. Since the Hamiltonian dynamics are reversible, at inference time, we randomly sample a choice of frame t and use forward and backward action of Hamiltonian to trace the trajectory of states after and before that frame for the respective action as stated in Equation 5.

For a sequence $\mathbf{x}_{1:T}$, we use the process in (6) to draw samples from a variational distribution $q(\mathbf{z}, \mathbf{s}_t | \mathbf{x}_{1:T}, \mathbf{u})$. Simply, we sample the content variable \mathbf{z} conditioned on the observed data and independently sample the motion states $\mathbf{s}_t^k = [\mathbf{q}_t^k, \mathbf{p}_t^k]$ for the reference frame t conditioned on the observed data and the relevant action k . Motion states corresponding to other actions are set to zero. In equations, this is,

$$\mathbf{z} \sim q(\mathbf{z} | \mathbf{x}_{1:T}), t \sim \mathcal{U}(\{1, \dots, T\}), \mathbf{q}_t^k \sim q(\mathbf{q}_t^k | \mathbf{x}_t, \mathbf{u}), \mathbf{p}_t^k \sim q(\mathbf{p}_t^k | \mathbf{x}_{t-w:t}, \mathbf{u}), \mathbf{s}_t^k = [\mathbf{q}_t^k, \mathbf{p}_t^k] \quad (6)$$

where t is a starting index, $q(\mathbf{q}_t^k | \mathbf{x}_t, \mathbf{u})$ is the posterior distributions of k^{th} position subspace conditioned on the frame \mathbf{x}_t and action variable \mathbf{u} , $q(\mathbf{p}_t^k | \mathbf{x}_{t-w:t}, \mathbf{u})$ is the posterior distributions of k^{th} momentum subspace conditioned on w previous frames and action variable \mathbf{u} and $q(\mathbf{z} | \mathbf{x}_{1:T})$ is the posterior distribution of the content space conditioned on the entire sequence. We parameterise the factorised posterior as a spherical Gaussian distribution learned using an encoder neural network. Specifically, $q(\mathbf{z} | \mathbf{x}_{1:T})$ as a content network, $q(\mathbf{q}_t^k | \mathbf{x}_t, \mathbf{u})$ as a position network, and $q(\mathbf{p}_t^k | \mathbf{x}_{t-w:t}, \mathbf{u})$ as a momentum network. We use reparametrisation trick (Kingma and Welling, 2013) to sample from latent distribution $\mathbf{z} = \boldsymbol{\mu} + \boldsymbol{\sigma} \odot \boldsymbol{\epsilon}$ where $\boldsymbol{\epsilon} \sim \mathcal{N}(0, \mathbf{I})$.

Learning Objective The learning problem reduces to the optimisation of the following objective,

$$\max -KL[q(\mathbf{q}_t^k | \mathbf{x}_t, \mathbf{u}) || p(\mathbf{q}_t^k)] - KL[q(\mathbf{p}_t^k | \mathbf{x}_{t-w:t}, \mathbf{u}) || p(\mathbf{p}_t^k)] - KL[q(\mathbf{z} | \mathbf{x}_{1:T}) || p(\mathbf{z})] + \mathbb{E}_{q(\mathbf{q}_t^k | \mathbf{x}_t, \mathbf{u})} \left[\sum_{t'} \log p(\mathbf{x}_{t'} | \mathbf{q}_{t'}, \mathbf{z}) \right].$$

We have provided the derivation of ELBO in Appendix ???. Figure 1, right side, is the probabilistic graph of the generative and inference model.

4 Experiments

The implementation details of neural network architecture and training procedure are discussed in Appendix ???. Our code is available on GitHub.² We first demonstrate the application of *HALO* on disentangling content and motion in sequences of rotating balls evolving under constant energy. Next, we investigate the applicability of our approach on two complex datasets: Sprites and MUG Aifanti et al. (2010).

Rotating Balls We construct a set of sequences of images of a ball that moves in an orbit under constraint $i^2 + j^2 = c$, where (i, j) is a centre of a ball and c is the distance from the centre of an

²<https://github.com/MdAsifKhan/HALO.git>

orbit. Each sequence is drawn from a different initial condition decided uniformly at random, and all sequences are of length 16. To introduce the content element, we colour half of the sequence as “red” and the remaining as “blue”. In Figure 3, we show the result of swapping the content variable of two held-out sequences that demonstrates the effectiveness of *HALO* in disentangling *motion* from the *content* while keeping the dynamics intact.

Next, we introduce details of the two datasets, followed by a discussion of the results in Section 4.1. **Sprites** is a sequence of animated characters performing different actions (‘walking’, ‘spell cast’ and ‘slashing’ from three viewing angles ‘left’, ‘right’ and ‘straight’) as per sprites sheets.³ The sequences are of length 8 RGB images of size $64 \times 64 \times 3$. Each character’s appearance has four attributes: skin colour, hairstyle, tops and pants. Each attribute can take six values resulting in 1296 unique characters. We used 1000 characters for training and the rest for evaluation. **MUG** (Aifanti et al., 2010) a dataset of six facial expressions (anger, disgust, fear, happiness, sadness and surprise) of 52 individuals. Sequences are of variable lengths ranging from 50 to 160 frames. We downsample the sequences by a factor of two and then take a random subsequence of length 8, crop the face region and resize it to 64×64 . The training and evaluation splits are based on (Tulyakov et al., 2018). We also demonstrate the application of our model in predicting rotations on MNIST digits where the symplectic structure proves useful for sampling long trajectories in the latent space. We refer to Appendix ?? for results.

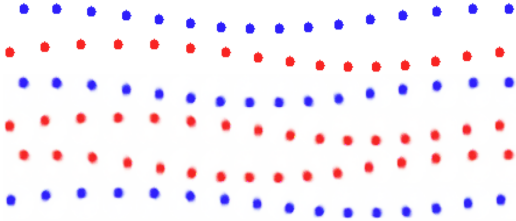


Figure 3: First two rows are original sequences, the next two rows are respective reconstructions, and the last two rows are generated by swapping the content variables. Swapping the content changes the colour but the dynamics are intact.

4.1 Results and Discussion

We first compare two choices of Hamiltonian structure, a symplectic group using \mathbf{H} and the symplectic orthogonal group by restricting \mathbf{H} to a skew-symmetric form that we refer to as skew- \mathbf{H} . Here, we map a starting frame to the latent space, unroll the trajectory and then map the timesteps to a data space using a decoder. We generate sequences of length 16 (twice the length used for training purposes). The sprites consist of periodic sequences of length 8 where the start and end frames are identical; in this case, we duplicate the sequence to get a ground truth of length 16. For MUG, we draw a sequence of length 16 from the evaluation set. We compare the generated sequences with target sequences using per-frame structural similarity index measure (SSIM), peak signal-to-noise ratio (PSNR) and mean squared error (MSE). The SSIM scores are between -1 and 1 , with a more significant score indicating more similarity between the ground truth and generated sequence. Likewise, higher PSNR and lower MSE imply better generation. Table 1 describes the performance under different scores, demonstrating our model can generate high-quality sequences from an input image. We observe that \mathbf{H} performs better than skew- \mathbf{H} . We hypothesise that the superior performance of \mathbf{H} can be attributed to the fact that skew- \mathbf{H} introduces additional restrictions on the parameters of \mathbf{H} that might be reducing the expressiveness of the model. This result is an interesting finding—the question we wish to investigate in future work. For the rest of the paper, we consider the dynamical operator \mathbf{H} .

Model	Dataset	SSIM \uparrow	PSNR \uparrow	MSE \downarrow
\mathbf{H}	Sprites	0.982 ± 0.005	36.76 ± 1.096	0.0005 ± 0.0002
	MUG	0.797 ± 0.003	24.49 ± 0.099	0.0040 ± 0.0001
Skew- \mathbf{H}	Sprites	0.950 ± 0.021	33.88 ± 2.03	0.0026 ± 0.0012
	MUG	0.791 ± 0.003	24.25 ± 0.094	0.0044 ± 0.0001

Table 1: We can see both choices of an operator can generate sequences close to the ground truth.

To evaluate disentanglement we compare with the state-of-the-art baselines DSVAE (Yingzhen and Mandt, 2018), MoCoGAN(Tulyakov et al., 2018) and S3VAE (Zhu et al., 2020).

Quantitative Evaluation We use a pretrained action prediction classifier for evaluating disentanglement. The architecture is provided in Table ?? of Appendix. To begin with, we draw a starting position and momentum from a prior distribution and use a dynamical model to unroll the trajectory in the phase space. Next, we sample the content variable \mathbf{z} from real sequences and combine it

³<https://github.com/jrconway3/Universal-LPC-spritesheet>

Method	Data	Accuracy \uparrow	$H(\mathbf{y} \mathbf{x})\downarrow$	$H(\mathbf{y})\uparrow$	IS \uparrow
<i>HALO</i> (conditional)		0.929	0.108	1.778	5.312
<i>HALO</i> (unconditional)		0.750	0.187	1.762	4.830
DSVAE (Yingzhen and Mandt, 2018)	MUG	0.543	0.374	1.657	3.607
MoCoGAN (Tulyakov et al., 2018)		0.631	0.183	1.721	4.655
S3VAE (Zhu et al., 2020)		0.705	0.135	1.760	5.078
<i>HALO</i> (conditional)		1.000	0.011	2.009	7.374
DSVAE (Yingzhen and Mandt, 2018)	Sprites	0.907	0.072	2.192	8.331
MoCoGAN (Tulyakov et al., 2018)		0.928	0.090	2.192	8.182
S3VAE (Zhu et al., 2020)		0.994	0.041	2.197	8.636

Sprites (Attr.)	Accuracy \uparrow
Skin Color	0.925
Shirt	0.948
Pant	0.968
Hair	0.992
Identity (MUG)	0.998

Table 2: Left shows the disentanglement of content and motion components of latent space. The high score of accuracy and Inter-Entropy $H(\mathbf{y})$ while low scores of Intra-Entropy $H(\mathbf{y}|\mathbf{x})$ are expected from a better model. Our model performs best across all three scores on MUG. On sprites, we are comparable to S3VAE. This is due to the simplicity of classes in sprites. We want to remark our unconditional model, as demonstrated on MUG, significantly outperforms other baselines showing the benefit of Hamiltonian even when labels are not available. On the right, we investigate the extent to which content is preserved when we switch motion variables with an arbitrary sequence. We report the accuracy of individual attributes in sprites and the identity of actors in the MUG dataset. The results show the content space can capture attributes that don’t change under dynamics.

with position variables to generate image sequences. We report the performance of the classifier in predicting the action from these generated sequences. The score is a useful measure of the model’s tendency to keep the motion intact with the modified content. We use the same classifier to report the intra-Entropy $H(\mathbf{y}|\mathbf{x})$ and inter-Entropy $H(\mathbf{y})$ that estimates the diversity of generated sequences. $H(\mathbf{y}|\mathbf{x})$ measures the closeness of generated sequences to the real sequences, and $H(\mathbf{y})$ measures the diversity of generated sequences (He et al., 2018). The two scores can be combined together to obtain inception score (IS) Salimans et al. (2016) a commonly used evaluation criterion for the diversity of generated samples ($\text{IS} = \exp(H(\mathbf{y}) - H(\mathbf{y}|\mathbf{x}))$ Barratt and Sharma (2018)). The results are reported in Table 2. We observe *HALO* outperforms the baselines on the MUG and is comparable with S3VAE on sprites. This improvement results from explicitly associating an action with a unique subspace that allows separability of the dynamics and avoids any mixing or ambiguity of action in the motion space. The results on sprites are comparable; we attribute this to the simplicity of sprites’ classes that result in high performance across all models. We want to remark that our formulation is not constrained by action variables \mathbf{u} . Table 2 also describes the results for an unconditional version on the MUG (Aifanti et al., 2010) that significantly outperforms the baseline. The details of the unconditional model are provided in Appendix ?? . The benefit of incorporating action variables \mathbf{u} is that it allows controlled generation of sequences, as demonstrated in Figure 6.

We, next evaluate the tendency to preserve the identity of sequences. For sprites, identity refers to four different attributes, and for MUG (Aifanti et al., 2010) it is the sequence label of the individual. We pre-train a classifier on the task of identity prediction and use it for evaluating the generated sequences. This way, we measure the model’s ability to keep the identity intact when the motion is changed. For sprites, we report the accuracy of individual attributes. Table 1 outlines the results. We can see on MUG that our model can preserve the identity with high accuracy. We can make a similar observation for different attributes of sprites sequences. Thus, good performance indicates that the content is preserved when traversing the motion subspace, and the motion space is invariant when changing the content variables. Also validated by the qualitative results.

Qualitative Evaluation We first evaluate the quality of sequence prediction by comparing the original sequence, its reconstruction and the generation from an initial frame. To predict the future timesteps of a sequence, we apply the motion operator on the latent encoding of the first time step. Figure 4 on the left are the results for sprites, and on the right of MUG video sequences. Next, we report sequences reconstructed by swapping motion variables to evaluate disentanglement. We start by encoding two sequences $\mathbf{x}_{1:T}^1$ and $\mathbf{x}_{1:T}^2$ to their latent representations $(\mathbf{z}^1, \mathbf{q}_{1:T}^1)$ and $(\mathbf{z}^2, \mathbf{q}_{1:T}^2)$, next we swap the motion variables $(\mathbf{z}^1, \mathbf{q}_{1:T}^1)$ and $(\mathbf{z}^2, \mathbf{q}_{1:T}^2)$ between the two representation spaces, and then pass the resulting representations through the decoder to generate the sequences $\mathbf{x}_{1:T}^{1\rightarrow 2}$ and $\mathbf{x}_{1:T}^{2\rightarrow 1}$. Figure 5, on the left, are the pair of consecutive rows of original sequences and on the right of the sequences generated by swapping the motion representations. We can see that swapping the motion part does not affect the identity of the sequences.

We now evaluate the image-to-sequence task to investigate the suitability of our model for a controlled generation. We first encode the image to its content and phase space coordinate in different motion spaces. Next, use the respective operators to unroll the trajectories in phase space, which are combined

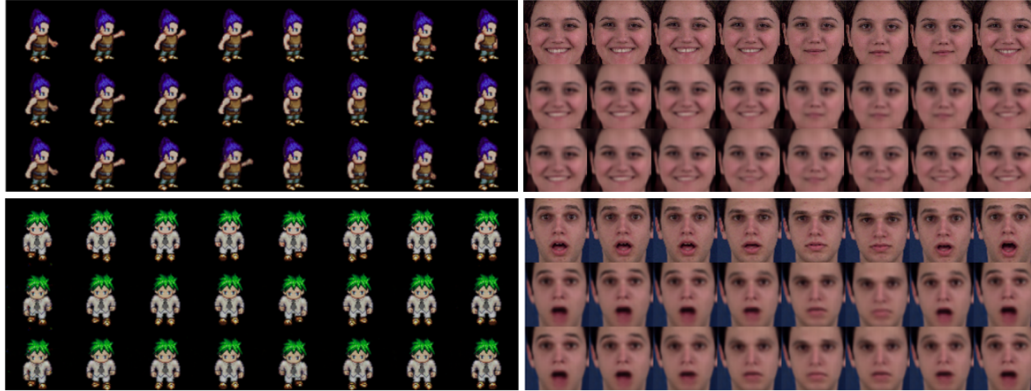


Figure 4: In each patch, the first row is the original sequence, the second row is reconstruction, and the third row is a sequence generated by an action of the operator on the starting time step. The reconstruction demonstrates our model can learn good representations, and the generation demonstrates the dynamical operator can capture realistic motions from an arbitrary starting frame. More examples are in Appendix ??



Figure 5: Qualitative demonstration of content and motion disentanglement. On the left side, we show rows of original sequence pairs and on the right are the reconstructions after swapping the motion variables in the latent space. More examples are in Appendix ??

with content and mapped to the image space using a decoder network. Figure 6 shows examples of decoding different motions from the same input image. For sprites, the actions are in order ‘walk’, ‘spell card’, ‘slash’ and for MUG they are ordered ‘anger’, ‘disgust’, ‘fear’, ‘happiness’, ‘sadness’ and ‘surprise’. We observe that the visual dynamics associated with all the operators are well separated. We also evaluate our model for long-term sequence generation; results are presented in Appendix ??, where it is apparent that longer-term sequences maintain the consistency associated with the content-motion pair.

Ablation We carry out ablation to identify the benefits of using *HALO* over other dynamical methods. Figure 6 we compare the motion transfer by replacing Hamiltonian with a linear dynamical model and RNN. We observe that, unlike *HALO*, the variations in dynamics get constant for Linear and RNN models. This result shows the benefit of Hamiltonian dynamics as, by definition, they ensure the phase space coordinates change over time, preventing the encoder neural network from channelling any static information in the motion space, which is vital for explicit disentanglement of content and motion variables. More results are provided in Appendix ?. We outline the key findings in Table 3. In Figure ?? of the appendix, we show the caveat with other dynamical models on the controlled generation task.

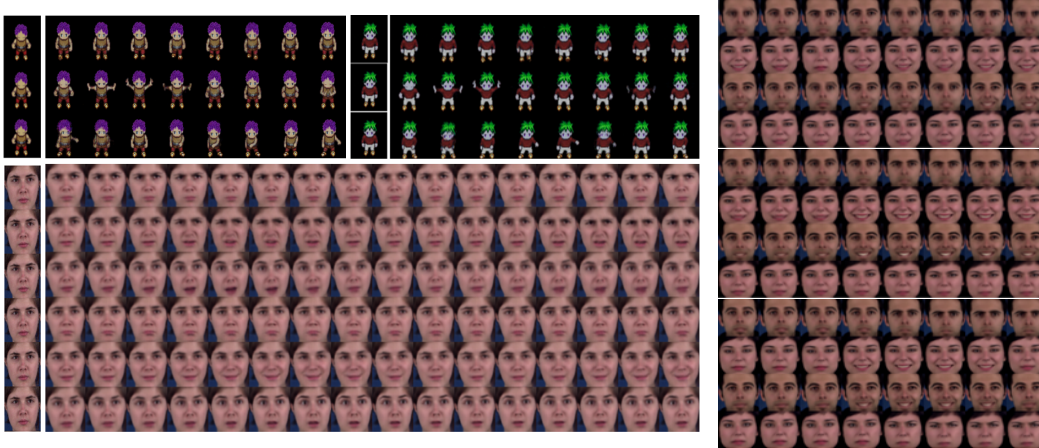


Figure 6: Left: examples of sequences generated by an action of Hamiltonian operator on the phase space representation of the starting frame. We observe that all dynamics are well separated, demonstrating the disentanglement of different actions. This result shows the benefit of the symplectic structure in motion space. Right: we demonstrate that our method outperforms other dynamical model baselines used for disentanglement. In each patch, rows one and two are original and rows three and four are obtained by swapping the motion components of latent space. The top is a Linear Model, the centre is RNN, and the last is *HALO*.

Our formulation proves useful for learning disentangled representations outperforming various baselines. We demonstrated its use for the controlled generation of image sequences. The effectiveness of our approach is a direct consequence of the *symplectic* geometry in the phase space, which prevents trajectories from deviating from the motion manifold. The choice of the quadratic form of energy provides a relationship among latent components, which we speculate is critical for the interpretability of actions.

Dynamics	Image-To-Seq.	Motion Swap	Structure
<i>HALO</i>	✓	✓	Symplectic
Linear	✗	✓	✗
RNN	✗	✓	✗
Positional Encoding	✗	✗	✗

Table 3: The benefits of our formulation over other dynamical models. The details on positional encoding are provided in Appendix ??.

5 Conclusions and Future Work

We introduced *HALO* – a DGM to disentangle motion from the content in image sequences. Our formulation utilises Hamiltonian latent operators to associate conserved quantities with the dynamics. Moreover, by the definition of the Hamiltonian dynamics, the motion space has to vary over time; this prevents the encoder neural network from channelling static information in the motion variables and therefore provides a helpful notion of disentanglement of content and motion. Our quantitative results with both conditional and unconditional models outperform the existing baselines. We furthermore demonstrate disentanglement qualitatively using motion swapping. In the conditional model, we associate every action with a unique Hamiltonian that proves critical for the controlled generation task of an image-to-sequence generation. *HALO* can generate long-term trajectories and traverse the motion manifolds of different actions in the latent space. We look forward to future applications to other sequential data types, such as molecular trajectories. A potential limitation of our model is that it is less able to deal with irregularly sampled sequences, changes in tempo or reversals. In future work, we wish to address this issue by allowing a more flexible prior on the spacing between time steps.

Societal Impact The applications of generative models for the realistic generation of images or videos is an immediate concern for society. The proposed application, like motion swap and controlled generation of videos, can be potentially misused for generating fake data. We restrict our paper’s scope to research and use data within the condition in the license agreement.

Acknowledgements

The authors would like to thank Joseph Mellor and William Toner for the helpful discussion during the project and Elliot J. Crowley for the valuable feedback on the paper. This research was funded in part by an unconditional gift from Huawei Noah’s Ark Lab, London.

Checklist

Please do not modify the questions and only use the provided macros for your answers. Note that the Checklist section does not count towards the page limit. In your paper, please delete this instructions block and only keep the Checklist section heading above along with the questions/answers below.

1. For all authors...
 - (a) Do the main claims made in the abstract and introduction accurately reflect the paper's contributions and scope? [Yes]
 - (b) Did you describe the limitations of your work? [Yes] In section 5
 - (c) Did you discuss any potential negative societal impacts of your work? [Yes] After conclusion.
 - (d) Have you read the ethics review guidelines and ensured that your paper conforms to them? [Yes]
2. If you are including theoretical results...
 - (a) Did you state the full set of assumptions of all theoretical results? [N/A]
 - (b) Did you include complete proofs of all theoretical results? [Yes] Provided derivation of ELBO in appendix.
3. If you ran experiments...
 - (a) Did you include the code, data, and instructions needed to reproduce the main experimental results (either in the supplemental material or as a URL)? [No] Data is publicly available and we provide github link to the code.
 - (b) Did you specify all the training details (e.g., data splits, hyperparameters, how they were chosen)? [Yes] All training details provided in appendix.
 - (c) Did you report error bars (e.g., with respect to the random seed after running experiments multiple times)? [Yes] We report error bars in Table 1.
 - (d) Did you include the total amount of compute and the type of resources used (e.g., type of GPUs, internal cluster, or cloud provider)? [Yes] In the appendix.
4. If you are using existing assets (e.g., code, data, models) or curating/releasing new assets...
 - (a) If your work uses existing assets, did you cite the creators? [Yes]
 - (b) Did you mention the license of the assets? [Yes] Provided link to obtain license of MUG dataset.
 - (c) Did you include any new assets either in the supplemental material or as a URL? [Yes] We provide details of our network, implementation additional results in supplementary. We provide such references in the paper.
 - (d) Did you discuss whether and how consent was obtained from people whose data you're using/curating? [N/A]
 - (e) Did you discuss whether the data you are using/curating contains personally identifiable information or offensive content? [Yes] There is no offensive content. The data of face images used in experiments is available from license by an external organisation. We provide reference to the concerned paper.
5. If you used crowdsourcing or conducted research with human subjects...
 - (a) Did you include the full text of instructions given to participants and screenshots, if applicable? [N/A]
 - (b) Did you describe any potential participant risks, with links to Institutional Review Board (IRB) approvals, if applicable? [N/A]
 - (c) Did you include the estimated hourly wage paid to participants and the total amount spent on participant compensation? [N/A]

References

- Aifanti, N., Papachristou, C., and Delopoulos, A. (2010). The MUG facial expression database. In *11th International Workshop on Image Analysis for Multimedia Interactive Services WIAMIS 10*, pages 1–4. IEEE.
- Bader, P., Blanes, S., and Casas, F. (2019). Computing the matrix exponential with an optimized Taylor polynomial approximation. *Mathematics*, 7(12):1174.
- Barratt, S. and Sharma, R. (2018). A note on the inception score. *arXiv preprint arXiv:1801.01973*.
- Bengio, Y., Courville, A., and Vincent, P. (2013). Representation learning: A review and new perspectives. *IEEE transactions on pattern analysis and machine intelligence*, 35(8):1798–1828.
- Bird, A. and Williams, C. K. (2019). Customizing sequence generation with multi-task dynamical systems. *arXiv preprint arXiv:1910.05026*.
- Bondesan, R. and Lamacraft, A. (2019). Learning symmetries of classical integrable systems. *arXiv preprint arXiv:1906.04645*.
- Botev, A., Jaegle, A., Wirsberger, P., Hennes, D., and Higgins, I. (2021). Which priors matter? benchmarking models for learning latent dynamics.
- Caselles-Dupré, H., Garcia-Ortiz, M., and Filliat, D. (2019). Symmetry-based disentangled representation learning requires interaction with environments. *arXiv preprint arXiv:1904.00243*.
- Chen, R. T., Rubanova, Y., Bettencourt, J., and Duvenaud, D. (2018). Neural ordinary differential equations. *arXiv preprint arXiv:1806.07366*.
- Chevalley, C. (2016). *Theory of Lie Groups (PMS-8), Volume 8*. Princeton University Press.
- Chung, J., Kastner, K., Dinh, L., Goel, K., Courville, A., and Bengio, Y. (2015). A recurrent latent variable model for sequential data. *arXiv preprint arXiv:1506.02216*.
- Cohen, T. and Welling, M. (2014). Learning the irreducible representations of commutative Lie groups. In *International Conference on Machine Learning*, pages 1755–1763. PMLR.
- Connor, M. and Rozell, C. (2020). Representing closed transformation paths in encoded network latent space. In *Proceedings of the AAAI Conference on Artificial Intelligence*, volume 34, pages 3666–3675.
- Cranmer, M., Sanchez-Gonzalez, A., Battaglia, P., Xu, R., Cranmer, K., Spergel, D., and Ho, S. (2020). Discovering symbolic models from deep learning with inductive biases. *arXiv preprint arXiv:2006.11287*.
- Cremers, D. and Yuille, A. (2003). A generative model based approach to motion segmentation. In *Joint Pattern Recognition Symposium*, pages 313–320. Springer.
- Culpepper, B. J. and Olshausen, B. A. (2009). Learning transport operators for image manifolds. In *NIPS*, pages 423–431.
- Dandi, Y., Das, A., Singhal, S., Namboodiri, V., and Rai, P. (2020). Jointly trained image and video generation using residual vectors. In *Proceedings of the IEEE/CVF Winter Conference on Applications of Computer Vision*, pages 3028–3042.
- Dupont, E., Martin, M. B., Colburn, A., Sankar, A., Susskind, J., and Shan, Q. (2020). Equivariant neural rendering. In *International Conference on Machine Learning*, pages 2761–2770. PMLR.
- Easton, R. W. (1993). Introduction to Hamiltonian dynamical systems and the N-body problem (KR Meyer and GR Hall). *SIAM Review*, 35(4):659–659.
- Eastwood, C. and Williams, C. K. (2018). A framework for the quantitative evaluation of disentangled representations. In *International Conference on Learning Representations*.
- Elliott, R. J. and Krishnamurthy, V. (1999). New finite-dimensional filters for parameter estimation of discrete-time linear Gaussian models. *IEEE Transactions on Automatic Control*, 44(5):938–951.

- Fraccaro, M., Kamronn, S., Paquet, U., and Winther, O. (2017). A disentangled recognition and nonlinear dynamics model for unsupervised learning. *arXiv preprint arXiv:1710.05741*.
- Franceschi, J.-Y., Delasalles, E., Chen, M., Lamprier, S., and Gallinari, P. (2020). Stochastic latent residual video prediction. In *International Conference on Machine Learning*, pages 3233–3246. PMLR.
- Goodfellow, I. J., Pouget-Abadie, J., Mirza, M., Xu, B., Warde-Farley, D., Ozair, S., Courville, A., and Bengio, Y. (2014). Generative adversarial networks. *arXiv preprint arXiv:1406.2661*.
- Greydanus, S., Dzamba, M., and Yosinski, J. (2019). Hamiltonian neural networks. *arXiv preprint arXiv:1906.01563*.
- He, J., Lehrmann, A., Marino, J., Mori, G., and Sigal, L. (2018). Probabilistic video generation using holistic attribute control. In *Proceedings of the European Conference on Computer Vision (ECCV)*, pages 452–467.
- Higgins, I., Amos, D., Pfau, D., Racaniere, S., Matthey, L., Rezende, D., and Lerchner, A. (2018). Towards a definition of disentangled representations. *arXiv preprint arXiv:1812.02230*.
- Hochreiter, S. and Schmidhuber, J. (1997). Long short-term memory. *Neural computation*, 9(8):1735–1780.
- Hogg, D. (1983). Model-based vision: A program to see a walking person. *Image and Vision Computing*, 1(1):5–20.
- Hsieh, J.-T., Liu, B., Huang, D.-A., Fei-Fei, L., and Niebles, J. C. (2018). Learning to decompose and disentangle representations for video prediction. *arXiv preprint arXiv:1806.04166*.
- Hsu, W.-N., Zhang, Y., and Glass, J. (2017). Unsupervised learning of disentangled and interpretable representations from sequential data. *arXiv preprint arXiv:1709.07902*.
- Hurri, J. and Hyvärinen, A. (2003). Temporal and spatiotemporal coherence in simple-cell responses: a generative model of natural image sequences. *Network: Computation in Neural Systems*, 14(3):527–551. PMID: 12938770.
- Kalman, R. E. (1960). A new approach to linear filtering and prediction problems.
- Kannan, A., Jovic, N., and Frey, B. J. (2005). Generative model for layers of appearance and deformation. In *AISTATS*, volume 2005.
- Karl, M., Soelch, M., Bayer, J., and Van der Smagt, P. (2016). Deep variational Bayes filters: Unsupervised learning of state space models from raw data. *arXiv preprint arXiv:1605.06432*.
- Kingma, D. P. and Welling, M. (2013). Auto-encoding variational Bayes. *arXiv preprint arXiv:1312.6114*.
- Lake, B. M., Ullman, T. D., Tenenbaum, J. B., and Gershman, S. J. (2017). Building machines that learn and think like people. *Behavioral and brain sciences*, 40.
- Memisevic, R. (2012). On multi-view feature learning. *arXiv preprint arXiv:1206.4609*.
- Miladinović, Đ., Gondal, W., Schölkopf, B., Buhmann, J. M., and Bauer, S. (2019). Disentangled state space models: Unsupervised learning of dynamics across heterogeneous environments.
- Minderer, M., Sun, C., Villegas, R., Cole, F., Murphy, K., and Lee, H. (2019). Unsupervised learning of object structure and dynamics from videos. *arXiv preprint arXiv:1906.07889*.
- Noether, E. (1918). Invariant variation problems, gott.
- Pavlovic, V., Rehg, J. M., and MacCormick, J. (2000). Learning switching linear models of human motion. In *NIPS*, volume 2, page 4.
- Quessard, R., Barrett, T., and Clements, W. (2020). Learning disentangled representations and group structure of dynamical environments. *Advances in Neural Information Processing Systems*, 33.

- Rao, R. P. and Ruderman, D. L. (1999). Learning Lie groups for invariant visual perception. *Advances in neural information processing systems*, pages 810–816.
- Roweis, S. and Ghahramani, Z. (1999). A unifying review of linear Gaussian models. *Neural computation*, 11(2):305–345.
- Salimans, T., Goodfellow, I., Zaremba, W., Cheung, V., Radford, A., and Chen, X. (2016). Improved techniques for training gans. *Advances in neural information processing systems*, 29.
- Sanchez-Gonzalez, A., Bapst, V., Cranmer, K., and Battaglia, P. (2019). Hamiltonian graph networks with ODE integrators. *arXiv preprint arXiv:1909.12790*.
- Sanchez-Gonzalez, A., Godwin, J., Pfaff, T., Ying, R., Leskovec, J., and Battaglia, P. (2020). Learning to simulate complex physics with graph networks. In *International Conference on Machine Learning*, pages 8459–8468. PMLR.
- Sohl-Dickstein, J., Wang, C. M., and Olshausen, B. A. (2010). An unsupervised algorithm for learning Lie group transformations. *arXiv preprint arXiv:1001.1027*.
- Srivastava, N., Mansimov, E., and Salakhudinov, R. (2015). Unsupervised learning of video representations using LSTMs. In *International conference on machine learning*, pages 843–852. PMLR.
- Starner, T. and Pentland, A. (1997). Real-time American sign language recognition from video using hidden Markov models. In *Motion-based recognition*, pages 227–243. Springer.
- Storkey, A. and Williams, C. (2003). Image modeling with position-encoding dynamic trees. *IEEE Transactions on Pattern Analysis and Machine Intelligence*, 25(7):859–871.
- Toth, P., Rezende, D. J., Jaegle, A., Racanière, S., Botev, A., and Higgins, I. (2019). Hamiltonian generative networks. *arXiv preprint arXiv:1909.13789*.
- Tulyakov, S., Liu, M.-Y., Yang, X., and Kautz, J. (2018). MoCoGAN: Decomposing motion and content for video generation. In *Proceedings of the IEEE conference on computer vision and pattern recognition*, pages 1526–1535.
- Villegas, R., Yang, J., Hong, S., Lin, X., and Lee, H. (2017). Decomposing motion and content for natural video sequence prediction. *arXiv preprint arXiv:1706.08033*.
- Yildiz, C., Heinonen, M., and Lähdesmäki, H. (2019). ODE2VAE: Deep generative second order ODEs with Bayesian neural networks.
- Yingzhen, L. and Mandt, S. (2018). Disentangled sequential autoencoder. In *International Conference on Machine Learning*, pages 5670–5679. PMLR.
- Yoon, J., Jarrett, D., and van der Schaar, M. (2019). Time-series generative adversarial networks.
- Zhu, Y., Min, M. R., Kadav, A., and Graf, H. P. (2020). S3VAE: Self-supervised sequential VAE for representation disentanglement and data generation. In *Proceedings of the IEEE/CVF Conference on Computer Vision and Pattern Recognition*, pages 6538–6547.

Supplementary Material

1 Derivation of ELBO

We use maximum loglikelihood on sequence variables to derive the evidence lower bound (ELBO),

$$\begin{aligned}
\log p(\mathbf{x}_{1:T}|\mathbf{u}) &= \log \int p(\mathbf{x}_{1:T}, \mathbf{z}, \mathbf{s}_{1:T}|\mathbf{u}) d\mathbf{s}_{1:T} d\mathbf{z} \\
&= \log \int \frac{p(\mathbf{x}_{1:T}, \mathbf{z}, \mathbf{s}_{1:T}|\mathbf{u})}{q(\mathbf{z}, \mathbf{s}_t|\mathbf{x}_{1:T}, \mathbf{u})} q(\mathbf{z}, \mathbf{s}_t|\mathbf{x}_{1:T}, \mathbf{u}) d\mathbf{s}_{1:T} d\mathbf{z} \\
&\geq \int \log \left[\frac{p(\mathbf{x}_{1:T}, \mathbf{z}, \mathbf{s}_{1:T}|\mathbf{u})}{q(\mathbf{z}, \mathbf{s}_t|\mathbf{x}_{1:T}, \mathbf{u})} \right] q(\mathbf{z}, \mathbf{s}_t|\mathbf{x}_{1:T}, \mathbf{u}) d\mathbf{s}_{1:T} d\mathbf{z} \\
&\geq \mathbb{E}_{q(\mathbf{z}, \mathbf{s}_t|\mathbf{x}_{1:T}, \mathbf{u})} \log \left[\frac{p(\mathbf{x}_{1:T}, \mathbf{z}, \mathbf{s}_{1:T}|\mathbf{u})}{q(\mathbf{z}, \mathbf{s}_t|\mathbf{x}_{1:T}, \mathbf{u})} \right] \tag{1}
\end{aligned}$$

where $\mathbf{s}_t = [\mathbf{q}_t, \mathbf{p}_t]$. The joint distribution is factorised as,

$$p(\mathbf{x}_{1:T}, \mathbf{z}, \mathbf{s}_{1:T}|\mathbf{u}) = p(\mathbf{z})p(\mathbf{x}_1|\mathbf{q}_1, \mathbf{z}) \prod_{t=1}^{T-1} p(\mathbf{x}_{t+1}|\mathbf{q}_{t+1}, \mathbf{z})p(\mathbf{q}_{t+1}, \mathbf{p}_{t+1}|\mathbf{q}_t, \mathbf{p}_t, \mathbf{u}) \tag{2}$$

Since, we transform the starting latent state $\mathbf{s}_1 = [\mathbf{q}_1, \mathbf{p}_1]$ using a deterministic transformation $f(t, \mathbf{H}; \omega) = e^{\mathbf{H}}$ (where ω are the parameters of \mathbf{H} matrix), we can write our transition distribution as,

$$p(\mathbf{s}_{t+1}|\mathbf{s}_t, \mathbf{u}) = p(\mathbf{s}_t|\mathbf{s}_{t-1}, \mathbf{u}) \left| \frac{df}{ds_t} \right| = p(\mathbf{s}_t|\mathbf{s}_{t-1}, \mathbf{u}) e^{\text{Tr}(\mathbf{H})} = p(\mathbf{s}_1|\mathbf{u}) \prod_{t=1}^t e^{\text{Tr}(\mathbf{H})} \tag{3}$$

where Tr is the trace operator and $p(\mathbf{s}_1|\mathbf{u}) = p(\mathbf{q}_1|\mathbf{u})p(\mathbf{p}_1|\mathbf{u})$. The transition model is reversible; therefore, without loss of generality, we can replace a starting step 1 with any arbitrary t and unroll both forward and backwards. We next equate (3) in the generative model defined in (2) that reduces the factorisation to,

$$p(\mathbf{x}_{1:T}, \mathbf{z}, \mathbf{s}_{1:T}|\mathbf{u}) = p(\mathbf{z})p(\mathbf{x}_1|\mathbf{q}_1, \mathbf{z})p(\mathbf{q}_t|\mathbf{u})p(\mathbf{p}_t|\mathbf{u}) \prod_{t=1, \neq t}^{T-1} p(\mathbf{x}_{t'}|\mathbf{q}_{t'})e^{\text{Tr}(\mathbf{H})} \tag{4}$$

We factorise the variational distribution $q(\mathbf{z}, \mathbf{s}_t|\mathbf{x}_{1:T}, \mathbf{u})$ as,

$$q(\mathbf{z}, \mathbf{s}_t|\mathbf{x}_{1:T}, \mathbf{u}) = q(\mathbf{z}|\mathbf{x}_{1:T})q(\mathbf{q}_t|\mathbf{x}_t, \mathbf{u})q(\mathbf{p}_t|\mathbf{x}_{t-w:t}, \mathbf{u}), \quad \mathbf{s}_t = [\mathbf{q}_t, \mathbf{p}_t] \tag{5}$$

We now use the equations (5) and (4) to rewrite the ELBO as,

$$\mathbb{E}_{q(\mathbf{z}|\mathbf{x}_{1:T}), q(\mathbf{q}_t|\mathbf{x}_t, \mathbf{u}), q(\mathbf{p}_t|\mathbf{x}_{t-w:t}, \mathbf{u})} \log \left[\frac{p(\mathbf{z})p(\mathbf{q}_t|\mathbf{u})p(\mathbf{p}_t|\mathbf{u})p(\mathbf{x}_1|\mathbf{q}_1, \mathbf{z}) \prod_{t'=1, \neq t}^T p(\mathbf{x}_{t'}|\mathbf{q}_{t'}, \mathbf{z})e^{T\text{r}(\mathbf{H})}}{q(\mathbf{z}|\mathbf{x}_{1:T})q(\mathbf{q}_t|\mathbf{x}_t, \mathbf{u})q(\mathbf{p}_t|\mathbf{x}_{t-w:t}, \mathbf{u})} \right] \tag{6}$$

$$\begin{aligned}
&\mathbb{E}_{q(\mathbf{q}_t|\mathbf{x}_t, \mathbf{u})} \log \left[\frac{p(\mathbf{q}_t|\mathbf{u})}{q(\mathbf{q}_t|\mathbf{x}_t, \mathbf{u})} \right] + \mathbb{E}_{q(\mathbf{p}_t|\mathbf{x}_{t-w:t}, \mathbf{u})} \log \left[\frac{p(\mathbf{p}_t|\mathbf{u})}{q(\mathbf{p}_t|\mathbf{x}_{t-w:t}, \mathbf{u})} \right] + \mathbb{E}_{q(\mathbf{z}|\mathbf{x}_{1:T})} \log \left[\frac{p(\mathbf{z})}{q(\mathbf{z}|\mathbf{x}_{1:T})} \right] \\
&+ \mathbb{E}_{q(\mathbf{q}_t|\mathbf{x}_t, \mathbf{u})} \left[\sum_{t'} \log p(\mathbf{x}_{t'}|\mathbf{q}_{t'}, \mathbf{z}) \right] \tag{7}
\end{aligned}$$

The trace of the real-Hamiltonian matrix is zero we can therefore omit the term $Tr(\mathbf{H})$. Since, for each motion \mathbf{u}_k we associate a separate Hamiltonian \mathbf{H}_k that acts on a subspace \mathbf{S}^k , we can view the full state space \mathbf{S} as a partitions of symmetry groups $\mathbf{S} = \mathbf{S}_1 \oplus \dots \oplus \mathbf{S}_K$ where the Hamiltonian \mathbf{H} is in the block diagonal form $\mathbf{H} = \text{diag}(\mathbf{H}_1, \dots, \mathbf{H}_K)$. We, therefore, express the distributions in terms of the variables of their respective subspaces to obtain the final ELBO,

$$-KL[q(\mathbf{q}_t^k | \mathbf{x}_t, \mathbf{u}) || p(\mathbf{q}_t^k)] - KL[q(\mathbf{p}_t^k | \mathbf{x}_{t-w:t}, \mathbf{u}) || p(\mathbf{p}_t^k)] - KL[q(\mathbf{z} | \mathbf{x}_{1:T}, \mathbf{u}) || p(\mathbf{z})] \\ + \mathbb{E}_{q(\mathbf{q}_t^k | \mathbf{x}_t, \mathbf{u})} \left[\sum_{t'} \log p(\mathbf{x}_{t'} | \mathbf{q}_{t'}, \mathbf{z}) \right] \quad (8)$$

2 Background

In this section, we provide a short overview of the definitions relevant to the context of our work. The symmetry of an object is a transformation that leaves some of its properties unchanged. E.g., translation, rotation, etc. The study of symmetries plays a fundamental role in discovering the constants of physical systems. For instance, space translation symmetry means the conservation of linear momentum, and rotation symmetry implies the conservation of angular momentum. Groups are fundamental tools used for studying symmetry transformations. Formally we say,

Definition 1. A group G is a set with a binary operation $*$ satisfying the following conditions:

- closure under $*$, i.e., $x * y \in G$ for all $x, y \in G$
- there is an identity element $e \in G$, satisfying $x * e = e * x = x$ for all $x \in G$
- for each element $x \in G$ there exist an inverse $x^{-1} \in G$ such that $x * x^{-1} = x^{-1} * x = e$
- for all $x, y, z \in G$ the associative law holds i.e. $x * (y * z) = (x * y) * z$

The nature of the symmetry present in a system decides whether a group is discrete or continuous. A group is discrete if it has a finite number of elements. For e.g., a dihedral group D_2 generated using an e identity, r rotation by π , and f reflection along x-axis consists of finite elements $\{e, r, f, rf\}$. The group generators are a set of elements that can generate other group elements using the group multiplication rule. For D_2 the generators are $\{e, r, f\}$. A continuous group is characterised by the notion of infinitesimal transformation and is generally known as the Lie group.

Definition 2. A Lie group G is a group which also forms a smooth manifold structure, where the group operations under multiplication $G \times G \rightarrow G$ and its inverse $G \rightarrow G$ are smooth maps.

A group of 2D rotations in a plane is one common example of Lie group given by, $\mathbf{SO}(2) = \{R \in \mathbb{R}^{2 \times 2} | R^T R = I, \det(R) = 1\}$. $\mathbf{SO}(2)$ is a single parameter group simply given by a 2D rotation matrix $R(\theta) = \begin{pmatrix} \cos \theta & -\sin \theta \\ \sin \theta & \cos \theta \end{pmatrix}$.

Definition 3. A Lie algebra \mathfrak{g} of a Lie group G is the tangent space to a group defined at its identity element I with an exponential map $\text{exp} : \mathfrak{g} \rightarrow G$ and a binary operation $\mathfrak{g} \times \mathfrak{g} \rightarrow \mathfrak{g}$.

The structure of Lie groups is of much interest due to Noether's theorem, which states that a conservation law exists for any differentiable symmetry. In physics, such conservation laws are studied by identifying the Hamiltonian of the physical system (Easton, 1993). In this work, we look at two choices of Hamiltonians that form a symplectic group $Sp(2d)$ and symplectic orthogonal group $SpO(2d)$ structure.

Definition 4. A symplectic group $Sp(2d)$ is a Lie group formed by the set of real symplectic matrices defined as $Sp(2d) = \{\mathbf{H} \in \mathbb{R}^{2d \times 2d} | \mathbf{H}^T \mathbf{J} \mathbf{H} = \mathbf{J}\}$, where $\mathbf{J} = \begin{pmatrix} 0 & \mathbf{I}_d \\ -\mathbf{I}_d & 0 \end{pmatrix}$.

Definition 5. The Lie algebra \mathfrak{sp} of a symplectic group $Sp(2d)$ is a vector space defined by, $\mathfrak{sp} = \{\mathbf{H} \in \mathbb{R}^{2d \times 2d} | \mathbf{J} \mathbf{H} = (\mathbf{J} \mathbf{H})^T\}$

Definition 6. A symplectic orthogonal group $SpO(2d)$ is defined by restricting the Hamiltonian matrices to be of orthogonal form.



Figure 1: Unconditional Hamiltonian approach. On top, the first row is an original sequence, the second row is the reconstruction, and the third row is generated by an action of Hamiltonian on the phase space representation of the first frame in the sequence. On the bottom is an example of a motion swap, on the left side are two original motions and on the right side are sequences generated by swapping the motion variables.

Definition 7. A group action is a map $\circ : G \times \mathcal{X} \rightarrow \mathcal{X}$ iff (i) $e \circ x = x, \forall x \in \mathcal{X}$, where e is the identity element of G , (ii) $(g_1 \cdot g_2) \circ x = g_1 \cdot (g_2 \circ x), g_1, g_2 \in G, \forall x \in \mathcal{X}$ where \cdot is a group operation.

3 Experiment and Results

3.1 Network Architecture

The architecture of the encoder and decoder network is based on (Yingzhen and Mandt, 2018) also outlined in Table 3 and 4. We use the same network architecture for both sprites and the MUG dataset. The output of an encoder is fed to the content, position, and momentum network to get the variational distributions in \mathbf{Z} , \mathbf{Q} and \mathbf{P} space. Table 5 describes the architecture of the network. For the position and momentum network, the input action k is represented by a one-hot vector \mathbf{u} that takes one at index k and is zero elsewhere.

3.1.1 Training details

For MUG, we choose $|\mathbf{Z}| = 512$, $|\mathbf{Q}| = K \times 12$ and $|\mathbf{P}| = K \times 12$ and for sprites $|\mathbf{Z}| = 256$, $|\mathbf{Q}| = K \times 6$ and $|\mathbf{P}| = K \times 6$, where K is the number of actions. For sprites, $K = 3$ and for MUG $K = 6$. To train all our models, we use an Adam (Kingma and Ba, 2014) optimiser with a learning rate of $2e^{-4}$ and a batch size of 24. We use Pytorch (Paszke et al., 2019) for the implementation. The code will be made available on publication. We train all our models on Nvidia GeForce RTX 2080 GPUs.

3.2 Results and Discussion

We further provide extended qualitative samples of our model on the MUG and sprites dataset. Figure (6) shows results of conditional sequence generation, Figure (9) shows results of motion swapping. Figure (7, 8) further shows examples of image to sequence generation. We generate 16 frames in future conditioned on an initial starting frame. Next, we adapt our model to scenarios where action variables are \mathbf{u} not available.

Unconditional Dynamics In our formulation introduced in Section ??, we use the action variable \mathbf{u} to map the sequence to its respective phase space that allows the separability of dynamics and controlled generation of motion sequences. The choice to use action variables do not restrict the Hamiltonian dynamics; in this section, we adapt our formulation to sequences where action variables are not available. Specifically, we factorise the phase space into K symmetry groups where the

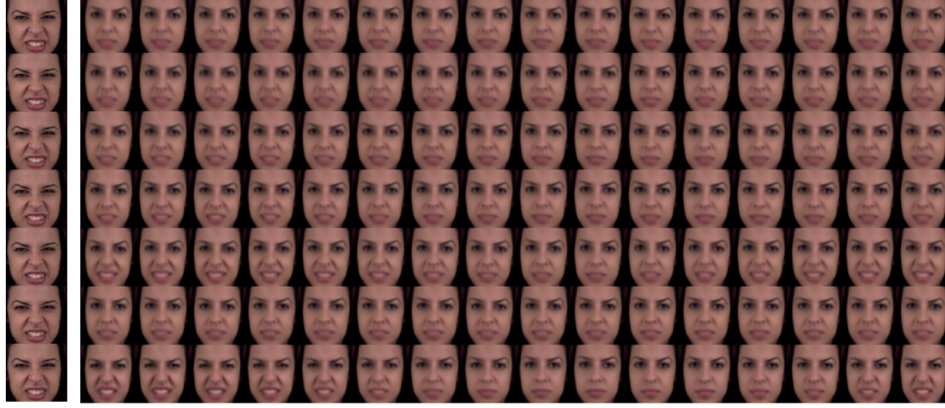


Figure 2: Unconditional Hamiltonian approach. An example of image-to-sequence generation. The first column is the starting frame, the first six rows correspond to the sequence generated by the action of $k - th$ block of \mathbf{H} , and the last row is the sequence generated by the full \mathbf{H} .

Hamiltonian takes the form $\mathbf{H} = \text{block-diagonal}(\mathbf{H}_1, \dots, \mathbf{H}_K)$. To unroll the trajectory for any arbitrary sequence $\mathbf{x}_{1:T}$ we evolve all the operators simultaneously as,

$$\mathbf{s}_t = f(\mathbf{s}_{t-1}^k; \omega_k, t) = \text{block-diagonal}(e^{t\mathbf{H}_1} \mathbf{s}_{t-1}^1, \dots, e^{t\mathbf{H}_K} \mathbf{s}_{t-1}^K) \quad \forall t > 1 \quad (9)$$

We want to remark that in such a formulation, we don't have direct control over the action generated by dynamics. The type of motion generated depends on the initial position and momenta variable. Furthermore, the operators \mathbf{H}_k may not necessarily correspond to specific action but could describe a more general property that is conserved and shared across motions. For instance, different operators could capture the varying magnitude of action movements like smiling, surprise, etc. To investigate it empirically, we map a starting frame to phase space and generate a sequence using individual \mathbf{H}_k as well as \mathbf{H} . Figure 2 describes the generated motion sequences. The first six rows are sequences generated by individual \mathbf{H}_k , and the combined \mathbf{H} generates the last row. We can observe the operators capture the varying extent of motion. Figure 1 further shows the performance of a model on sequence generation and motion transfer.

3.3 Ablation

To investigate the effectiveness of our dynamical model, we perform the following ablation studies,

What is the benefit of Constant Energy? The Hamiltonian formulation maintains the constant energy over time. Such a choice is beneficial for generating long-term sequences. In this part, we generate long sequences using our dynamical model and look at the evaluation of energy over time.

The total Hamiltonian energy in the phase space is given by,

$$\mathbf{E} = \frac{1}{2} \mathbf{s}^T \mathbf{M} \mathbf{s} \quad (10)$$

where $\mathbf{s} = (\mathbf{q}, \mathbf{p})$, and \mathbf{M} is a symmetric matrix. Let \mathbf{M} be a 2×2 block matrix $\mathbf{M} = \begin{pmatrix} \mathbf{A} & \mathbf{B} \\ \mathbf{B} & \mathbf{C} \end{pmatrix}$. We can expand the energy term as,

$$\mathbf{E} = \frac{1}{2} \mathbf{q}^T \mathbf{A} \mathbf{q} + \frac{1}{2} \mathbf{p}^T \mathbf{C} \mathbf{p} + \frac{1}{2} \mathbf{q}^T \mathbf{A} \mathbf{p} + \frac{1}{2} \mathbf{p}^T \mathbf{B} \mathbf{q} \quad (11)$$

The first term is potential energy (PE), the second is kinetic energy (KE), and the last two combined are non-separable terms. When \mathbf{B} is zero, the energy is entirely separable into KE and PE terms. The non-separable Hamiltonian is common in many physical problems, for instance, rigid body dynamics

and many others appearing in quantum mechanics. For details, we refer to Easton (1993). The choice of the unconstrained linear form of Hamiltonian was motivated to allow more flexibility to the model to learn in a data-driven way.

In Figure 3, we report the plot of energy over time for an image under different motion dynamics. The change in the individual energy shows the dynamics are not constant; this is also evident from the corresponding image sequences shown in the plot. As dynamics evolve, the total energy is strictly conserved, demonstrating that the trajectory cannot diverge from the learned symplectic structure. The results demonstrate the benefit of our model in generating long-term sequences. We want to add a remark that the energy terms should be interpreted with care. It might not have any equivalence to the energy of a physical system; what it does is that it provides constraints to use the time translation symmetry of the dynamics.

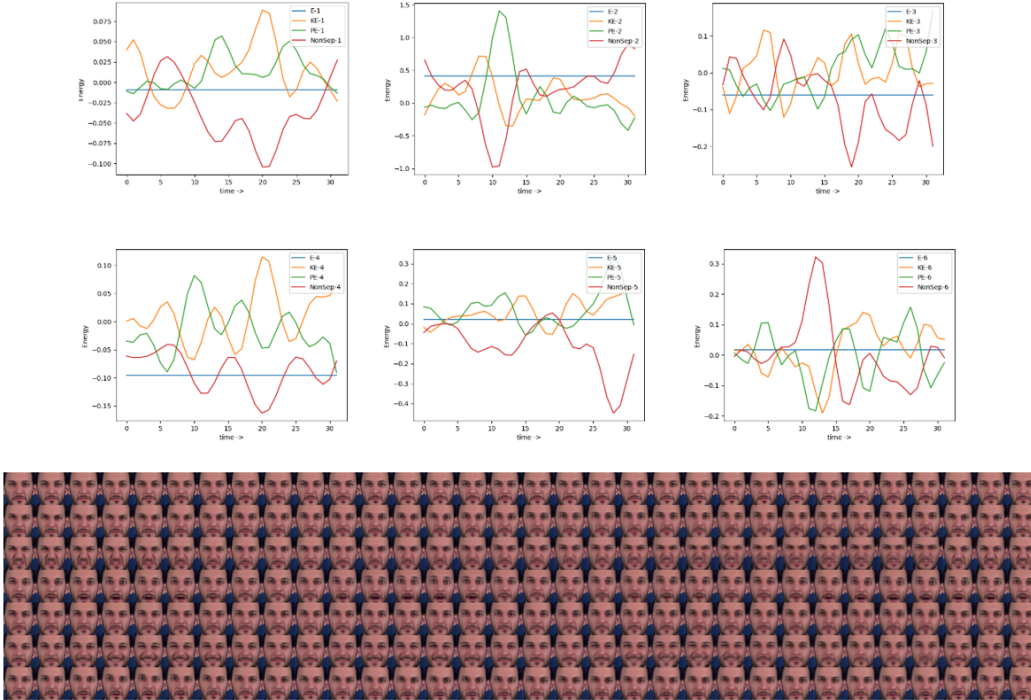


Figure 3: We map a starting frame to the phase space and use the operators \mathbf{H} to generate the phase space trajectory, which is then mapped to data space using the decoder network. At the top is the plot of energy vs time of the operators \mathbf{H}_k (E is the total energy, KE is the kinetic energy term, PE is the potential energy, and $Non.Sep$ is the non-separable term). Below, each row is the sequence generated by the action of \mathbf{H}_k .

Linear Model A linear dynamical is defined as,

$$\mathbf{h}_t = \mathbf{A}_{t-1}\mathbf{s}_{t-1} + \mathbf{B}_{t-1}\mathbf{h}_{t-1} + \mathbf{b} \quad (12)$$

where \mathbf{h}_t is a hidden state, and $\{\mathbf{A}, \mathbf{B}, \mathbf{b}\}$ are learnable parameters. To generate the trajectory $\mathbf{x}_{1:T}$, we combine the state coordinates $\mathbf{h}_{1:T} = \{\mathbf{h}_1, \dots, \mathbf{h}_T\}$ with the content variable \mathbf{z} and pass the joint representation through the decoder network. We report the performance of a linear model in conditional as well as unconditional settings.

Positional Encoding We generate a simplistic baseline using a fixed Fourier encoding representation. Specifically, for a sequence of frames $\mathbf{x}_{1:T} = \{\mathbf{x}_1, \dots, \mathbf{x}_T\}$ we map it to a content variable \mathbf{z} and a frame \mathbf{x}_t to a phase $\phi_t \in [-1, 1]$. We then generate $T - t$ linearly separated phase coordinates $\{\phi_t, \dots, \phi_T\} \in [\phi_t, 1 + \phi_t]$ and define the motion space representation as,

$$\mathbf{s}_t = \{\sin(\phi_t 2^k), \cos(\phi_t 2^k)\}_{k=1}^{\lfloor d/2 \rfloor} \quad (13)$$

where d is the size of motion space. We impose a Gaussian prior on the phase coordinates $p(\phi_t) = \mathcal{N}(0, 1)$.



(a) Linear Model



(b) RNN Model



(c) *Halo*

Figure 4: Results on Image to sequence generation. On the left is the starting frame and on the right are different motions generated by the dynamical models.

3.4 Discussion

In this section, we compare *Halo* with other choices of dynamical models. We describe the qualitative results in Table 1. The Hamiltonian model achieves the best performance across all scores. We observe all models except the position encoding achieve comparable performance on identity prediction. We speculate this could be due to the non-changing dynamics, which makes predicting the identity from a sequence of static images much easier for a classifier. Due to the failure of positional encoding, we omit it from the rest of the discussion. We restrict the qualitative analysis to conditional models. Figure 4 describes the results on image-to-sequence generation, further demonstrating that the Hamiltonian dynamics are consistent in long-term prediction and prevent the flow of constant information to motion variables. Overall the Hamiltonian formulation outperforms other approaches and works best across all tasks.

Method	Accuracy \uparrow	$\mathbf{H}(\mathbf{y} \mathbf{x})\downarrow$	$\mathbf{H}(\mathbf{y})\uparrow$	IS \uparrow
<i>HALO</i>	0.929	0.108	1.778	5.312
Linear	0.548	0.722	1.553	2.295
RNN	0.580	0.759	1.743	2.675
<i>HALO</i> (unconditional)	0.750	0.187	1.762	4.830
Linear (unconditional)	0.451	0.962	1.525	1.756
RNN (unconditional)	0.550	1.015	1.658	1.902
Positional Encoding	0.152	0.978	1.150	1.188

(a) Results of a classifier on MUG for different choices of dynamical models. The high score of accuracy and Inter-Entropy $\mathbf{H}(\mathbf{y})$ while low scores of Intra-Entropy $\mathbf{H}(\mathbf{y}|\mathbf{x})$ are expected from a better model.

Identity	Accuracy \uparrow
<i>HALO</i>	0.998
Linear	0.996
RNN	1.000
<i>HALO</i> (unconditional)	0.994
Linear (unconditional)	0.974
RNN (unconditional)	0.998
Positional Encoding	0.009

(b) Comparison to other baselines in terms of accuracy of the identity of sequences. This shows our model can preserve content when the motion representation is changed.

Table 1: Quantitative evaluation of disentanglement and diversity of generated samples

Model	MSE \downarrow
GPPVAE-dis (Casale et al., 2018)	0.0306
GPPVAE-joint (Casale et al., 2018)	0.0280
ODE ² VAE (Yildiz et al., 2019)	0.0204
ODE ² VAE-KL (Yildiz et al., 2019)	0.0184
<i>Halo</i> (Ours)	0.0208

Table 2: Mean squared error on test set of rotating MNIST.

3.5 Rotating MNIST

In this section, we investigate the performance of our approach in predicting the rotations of MNIST digits. We use an unconditional version of our model for this part. Following the procedure of Casale et al. (2018), we generated sequences of 16 time steps by rotating the images of digit “3”. We followed the same training procedure. In Figure 5, part (a) first row is the input sequence, and the second row is a reconstruction. In part (b), we show three sequences generated by random initial phase space coordinates. The network architecture for MNIST experiments is outlined in the Table (6, 7, 8).

Next, in Table 2, we compare the mean squared error (MSE) of our model with the other related methods (Yildiz et al., 2019; Casale et al., 2018). Our model achieves comparable performance to GPPVAE. The ODE²VAE performs best in terms of MSE; this can be attributed to using a second-order latent ODE model. In contrast, our formulation only uses first-order dynamics, which provides extra computational efficiency. Furthermore, compared to GPPVAE, we don’t have costly kernel computations.

We want to remark datasets such as stochastic movingMNIST Denton and Birodkar (2017) used in a few disentanglement papers is not a good application of our model. This is due to the nature of dynamics generated by an action of a random transformation. The Hamiltonian model relies on a dataset of data sequences where dynamics follow a conserved quantity and can be associated with constant energy. This assumption may or may not hold for SMNIST data due to random movements.

References

- Casale, F. P., Dalca, A. V., Saglietti, L., Listgarten, J., and Fusi, N. (2018). Gaussian process prior variational autoencoders. *arXiv preprint arXiv:1810.11738*.
- Denton, E. and Birodkar, V. (2017). Unsupervised learning of disentangled representations from video. In *Proceedings of the 31st International Conference on Neural Information Processing Systems*, pages 4417–4426.

Encoder Architecture of Sprites and MUG	
Conv2d	kernels: 256, kernelSize: (5, 5), stride: (1, 1), padding: (2, 2) BatchNorm2d → LeakyReLU(0.2)
Conv2d	kernels: 256, kernelSize: (5, 5), stride: (2, 2), padding: (2, 2) BatchNorm2d → LeakyReLU(0.2)
Conv2d	kernels: 256, kernelSize: (5, 5), stride: (2, 2), padding: (2, 2) BatchNorm2d → LeakyReLU(0.2)
Conv2d	kernels: 256, kernelSize: (5, 5), stride: (2, 2), padding: (2, 2) BatchNorm2d → LeakyReLU(0.2)
Conv2d	kernels: 256, kernelSize: (5, 5), stride: (1, 1), padding: (2, 2) BatchNorm2d → LeakyReLU(0.2) → Rearrange('b c w h -> b (c w h)')
Linear	in:=(c w h), out: 4096 BatchNorm1d → LeakyReLU(0.2)
Linear	in: 4096, out: 2048 BatchNorm1d → LeakyReLU(0.2)
Linear	in: 2048, out: h BatchNorm1d → LeakyReLU(0.2)

Table 3: Encoder network

Decoder Architecture of Sprites and MUG	
Linear	in: h , out: 4096 BatchNorm1d → LeakyReLU(0.2)
Linear	in: 4096, out:(c w h) BatchNorm1d → LeakyReLU(0.2) → Rearrange('b (c w h) -> b c w h')
ConvTranspose2d	kernels: 256, kernelSize: (5, 5), stride: (2, 2), padding: (2, 2) BatchNorm2d → LeakyReLU(0.2)
ConvTranspose2d	kernels: 256, kernelSize: (5, 5), stride: (2, 2), padding: (2, 2) BatchNorm2d → LeakyReLU(0.2)
ConvTranspose2d	kernels: 256, kernelSize: (5, 5), stride: (2, 2), padding: (2, 2) BatchNorm2d → LeakyReLU(0.2)
ConvTranspose2d	kernels: 256, kernelSize: (5, 5), stride: (2, 2), padding: (2, 2) BatchNorm2d → LeakyReLU(0.2)
ConvTranspose2d	kernels: 256, kernelSize: (5, 5), stride: (1, 1), padding: (2, 2) BatchNorm2d → Tanh()

Table 4: Decoder network

Content and Motion Architecture of Sprites and MUG					
Content		Position		Momentum	
LSTM	in: h , out: z	Linear	in: $h + k$, out: v	Linear	in: $h + k$, out: v
Linear $_{\mu}$	in: z , out: z	BatchNorm1d	→ LeakyReLU(0.2)	BatchNorm1d	→ LeakyReLU(0.2)
Linear $_{\log \sigma}$	in: z , out: z	Linear	in: v , out: v	Linear	in: v , out: v
		BatchNorm1d	→ LeakyReLU(0.2)	BatchNorm1d	→ LeakyReLU(0.2)
		Linear $_{\mu}$	in: v , out: q	TCN	kernelSize: 3, pad: 2, stride: 1
		Linear $_{\log \sigma}$	in: v , out: q	Linear $_{\mu}$	in: v , out: p
				Linear $_{\log \sigma}$	in: v , out: p

Table 5: Content and Motion network. TCN stands for temporal convolution network.

Encoder Architecture MNIST	
Conv2d	kernels: 32, kernelSize: (5, 5), stride: (2, 2), padding: (2, 2) BatchNorm2d → ReLU()
Conv2d	kernels: 64, kernelSize: (5, 5), stride: (2, 2), padding: (2, 2) BatchNorm2d → ReLU()
Conv2d	kernels: 128, kernelSize: (5, 5), stride: (2, 2), padding: (2, 2) BatchNorm2d → ReLU()
Linear	in: ($c \times w \times h$), out: 4096 BatchNorm1d → ReLU()
Linear	in: 4096, out: 256 BatchNorm1d → ReLU()

Table 6: Encoder network MNIST

Decoder Architecture MNIST	
Linear	in: 20, out: 4096 BatchNorm1d → ReLU()
Linear	in: 4096, out: ($c \times w \times h$) BatchNorm1d → ReLU() → Rearrange('b (c w h) -> b c w h')
ConvTranspose2d	kernels: 128, kernelSize: (3, 3), stride: (1, 1), padding: (0, 0) BatchNorm2d → ReLU()
ConvTranspose2d	kernels: 64, kernelSize: (5, 5), stride: (2, 2), padding: (1, 1) BatchNorm2d → ReLU()
ConvTranspose2d	kernels: 32, kernelSize: (5, 5), stride: (2, 2), padding: (1, 1) BatchNorm2d → ReLU()
ConvTranspose2d	kernels: 1, kernelSize: (5, 5), stride: (1, 1), padding: (2, 2) BatchNorm2d → Sigmoid()

Table 7: Decoder network MNIST

Motion Network MNIST			
Position		Momentum	
Linear	in: 256, out: 320	Linear	in: 256, out: 320
BatchNorm1d	→ LeakyReLU(0.2)	BatchNorm1d	→ LeakyReLU(0.2)
Linear	in: 320, out: 20	Linear	in: 320, out: 20
BatchNorm1d	→ LeakyReLU(0.2)	BatchNorm1d	→ LeakyReLU(0.2)
Linear _{μ}	in: 20, out: 20	TCN	kernelSize: 4, pad: 3, stride: 1
Linear _{$\log \sigma$}	in: 20, out: 20	Linear _{μ}	in: 20, out: 20
		Linear _{$\log \sigma$}	in: 20, out: 20

Table 8: Motion network MNIST. TCN stands for temporal convolution network.



Figure 5: Results on Rotating MNIST with a learnable Hamiltonian operator. On the top left, we have four input sequences, and on the right, their reconstruction; on the bottom, we have four sequences generated by an action of Hamiltonian on the state space coordinate of the frame in the first column.

Classifier Architecture	
Conv2d	kernels: 64, kernelSize: (5, 5), stride: (4, 4), padding: (1, 1) BatchNorm2d → LeakyReLU(0.2)
Conv2d	kernels: 128, kernelSize: (5, 5), stride: (4, 4), padding: (1, 1) BatchNorm2d → LeakyReLU(0.2)
Conv2d	kernels: 256, kernelSize: (5, 5), stride: (4, 4), padding: (1, 1) BatchNorm2d → LeakyReLU(0.2)
Linear	in: $(c \times w \times h)$, out: 1024 BatchNorm1d → LeakyReLU(0.2)
LSTM	in: 1024, out: 512 BatchNorm1d → LeakyReLU(0.2)
Linear	in: 512, out: 256 BatchNorm1d → LeakyReLU(0.2)
Linear	in: 256, out: K

Table 9: Classifier network used for evaluation. For the attribute classification task, K is set to the number of attributes and for the action classification, it is set to the number of actions.

Easton, R. W. (1993). Introduction to Hamiltonian dynamical systems and the N-body problem (KR Meyer and GR Hall). *SIAM Review*, 35(4):659–659.

Kingma, D. P. and Ba, J. (2014). Adam: A method for stochastic optimization. *arXiv preprint arXiv:1412.6980*.

Paszke, A., Gross, S., Massa, F., Lerer, A., Bradbury, J., Chanan, G., Killeen, T., Lin, Z., Gimelshein, N., Antiga, L., Desmaison, A., Kopf, A., Yang, E., DeVito, Z., Raison, M., Tejani, A., Chilamkurthy, S., Steiner, B., Fang, L., Bai, J., and Chintala, S. (2019). Pytorch: An imperative style, high-performance deep learning library. In Wallach, H., Larochelle, H., Beygelzimer, A., d'Alché-Buc, F., Fox, E., and Garnett, R., editors, *Advances in Neural Information Processing Systems 32*, pages 8024–8035. Curran Associates, Inc.

Yildiz, C., Heinonen, M., and Lähdesmäki, H. (2019). ODE2VAE: Deep generative second order ODEs with Bayesian neural networks.

Yingzhen, L. and Mandt, S. (2018). Disentangled sequential autoencoder. In *International Conference on Machine Learning*, pages 5670–5679. PMLR.



(a) Conditional Sequence Generation. The first row is the original sequence, the second row is a reconstructed sequence, and the third is generated by an action of a dynamical model on the first time frame

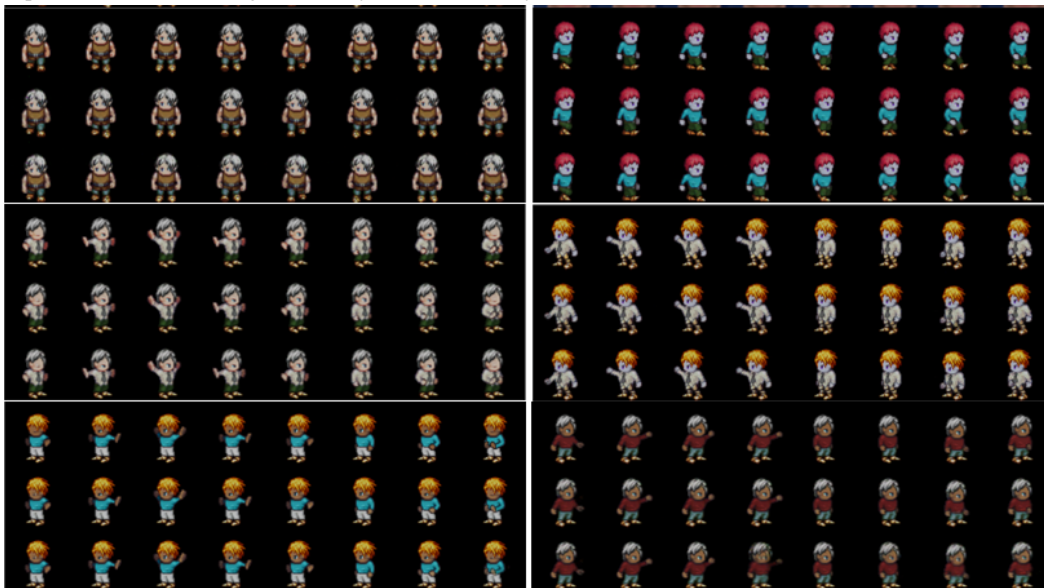


Figure 6: Conditional Sequence Generation. The first row is the original sequence, the second row is a reconstructed sequence, and third is generated by an action of a dynamical model on the first time frame

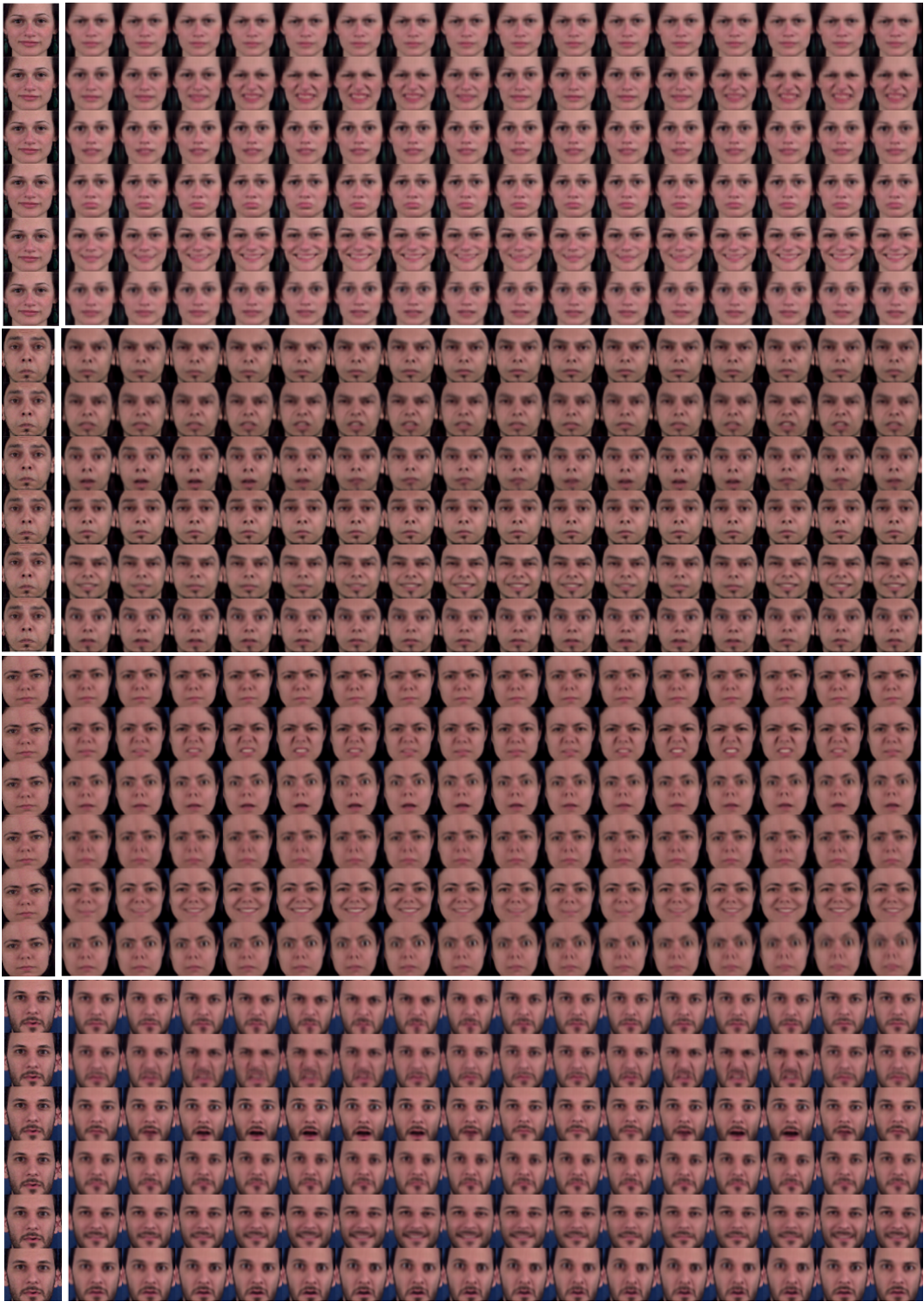


Figure 7: Image to Sequence generation. We generate dynamics of different actions from a given image. Each row is a unique action generated by the operator associated with that action.

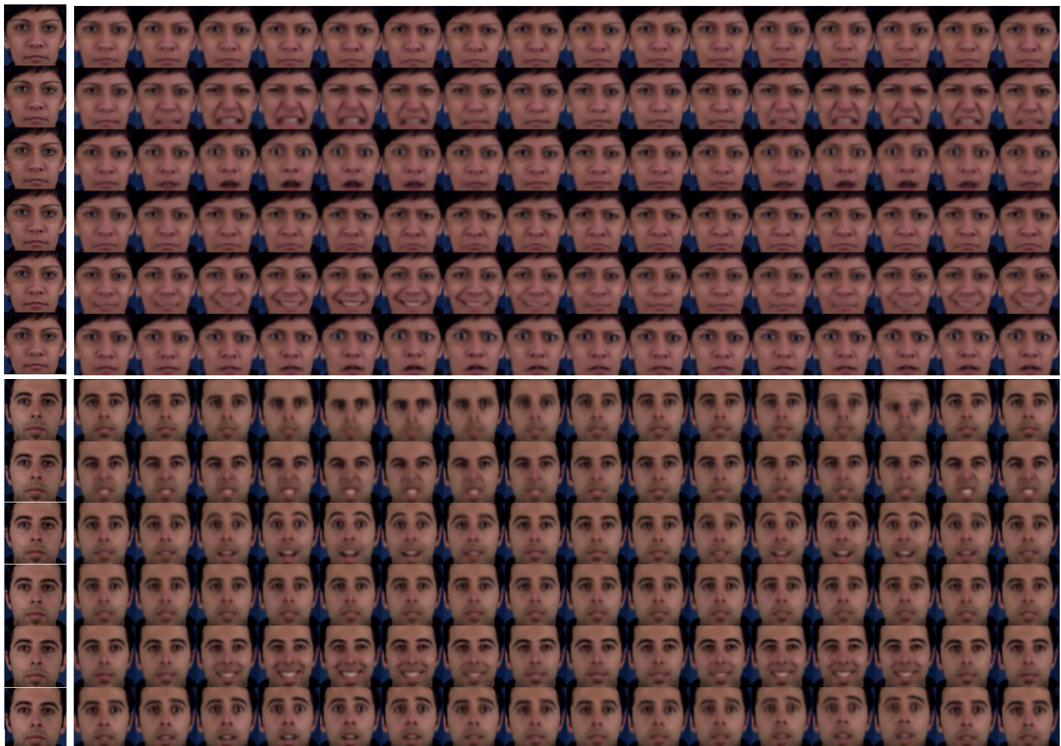


Figure 8: Image to Sequence generation. We generate dynamics of different actions from a given image. Each row is a unique action generated by the operator associated with that action.

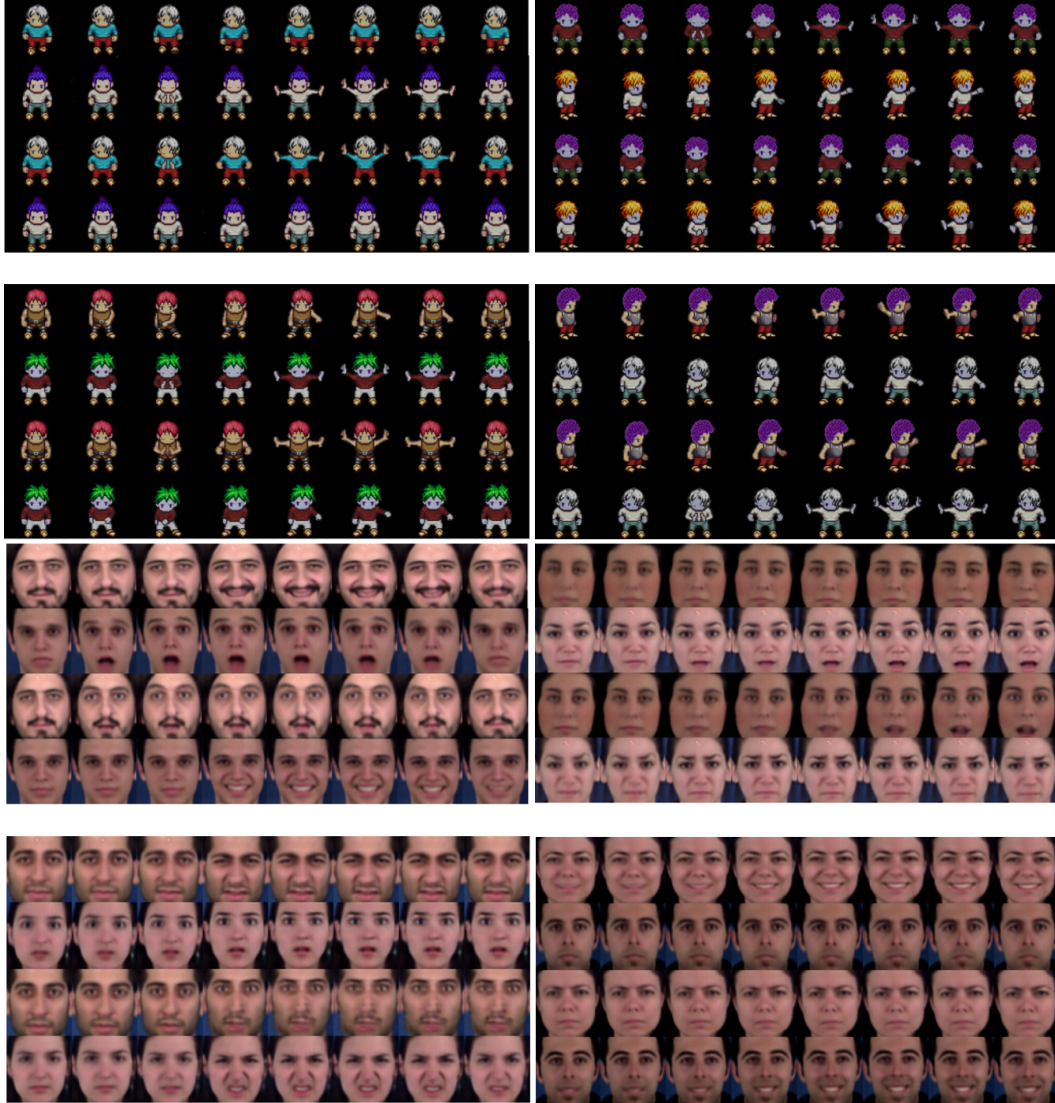


Figure 9: Motion Swapping. In each patch, the first two rows are the original sequence and the next two rows are obtained by swapping motion variables of two sequences.